INSTITUTO POTOSINO DE INVESTIGACIÓN CIENTÍFICA Y TECNOLÓGICA, A.C.

POSGRADO EN CIENCIAS EN BIOLOGÍA MOLECULAR

Microevolution of *Candida glabrata* in the presence of fluconazole

Tesis que presenta

Rosa Lilian Díaz Chávez

Para obtener el grado de

Maestra en Ciencias en Biología Molecular

Codirectores de la Tesis:

Dra. Irene Beatriz Castaño Navarro

Dr. Alejandro Juárez Reyes

San Luis Potosí, S.L.P., julio de 2024

Constancia de aprobación de la tesis

La tesis "**Microevolution of *Candida glabrata* in the presence of fluconazole**" presentada para obtener el Grado de Maestro(a) en Ciencias en Biología Molecular fue elaborada por **Rosa Lilián Díaz Chávez** y aprobada el **8 de julio de 2024** por los suscritos, designados por el Colegio de Profesores de la División de Biología Molecular del Instituto Potosino de Investigación Científica y Tecnológica, A.C.

_____	_____
Dra. Irene Beatriz Castaño Navarro	**Dr. Alejandro Juárez Reyes**
Codirectora de la tesis	Codirector de la tesis

_____

Dr. Rubén Hipólito López Revilla

Miembro del Comité Tutoral

Créditos Institucionales

Esta tesis fue elaborada en el Laboratorio de Microbiología Molecular de la División de Biología Molecular del Instituto Potosino de Investigación Científica y Tecnológica, A.C., bajo la codirección de la Dra. Irene Beatriz Castaño Navarro y el Dr. Alejandro Juárez Reyes.

Durante la realización del trabajo la autora recibió una beca académica del Consejo Nacional de Humanidades, Ciencias y Tecnologías No. 1241661 y del Instituto Potosino de Investigación Científica y Tecnológica, A. C.

Esta trabajo fue apoyado por el proyecto No. CF-2019-610281 del Consejo Nacional de Humanidades, Ciencias y Tecnologías, otorgado a Irene Beatriz Castaño Navarro.

Esta tesis contó con el apoyo del Laboratorio Nacional de Biotecnología Agrícola, Médica y Ambiental (LANBAMA), así como del Laboratorio de Microscopía para Muestras Biológicas de la División de Biología Molecular del IPICYT.

Acta de examen de grado

Página en Blanco que se va a utilizar para colocar la copia del acta de examen.

Dedicatorias

A todos aquellos que me dijeron que "sólo era escribir un poco más" y "falta poco": sus palabras de ánimo y apoyo fueron invaluables. Les dedico cada página, cada tabla y cada noche sin dormir. Aprecio mucho su optimismo y cariño.

Finalmente, a mis familiares y amigos, que aprendieron más de lo que jamás quisieron saber sobre mi tema de tesis, y que se memorizaron el speech "*Candida glabrata* es un hongo patógeno oportunista". Les aseguro que, en el siguiente proyecto, sólo habrá charlas sobre cosas más divertidas... como dicalcogenuros de metales de transición.

And last but not least, a mi cafetera, que fue mi compañera fiel en las noches más largas. Sin ti, esto no sería posible... o al menos, no tan rápido. Gracias por cada sorbo de energía y por nunca juzgarme por la cantidad de café que tomé.

Agradecimientos

Expreso mi más sincero agradecimiento al Instituto Potosino de Investigación Científica y Tecnológica por su invalorable apoyo institucional durante este trayecto académico.

Asimismo, mi reconocimiento al Consejo Nacional de Ciencia y Tecnología por beca otorgada para la realización de mis estudios de Maestría.

A la Dra. Irene Castaño Navarro, mi profunda gratitud por su dedicación al guiarme y enseñarme en este proyecto. Su ejemplo como científica y persona ha sido inspirador.

Al Dr. Alejandro Juárez Reyes, agradezco sinceramente su orientación, apoyo, vasto conocimiento y paciencia que me brindó en cada etapa de este trabajo.

Al Dr. Alejandro De Las Peñas, mi reconocimiento por sus valiosas enseñanzas, ideas y sugerencias que contribuyeron significativamente a este proyecto.

El Dr. Rubén Hipólito López Revilla merece mi agradecimiento por sus valiosos comentarios, sugerencias y apoyo que enriquecieron este trabajo.

A la Dra. Guadalupe Gutiérrez Escobedo por el apoyo técnico brindado y la enseñanzas impartidas.

A la Dra. Olga Araceli Patrón Soberano por su invaluable colaboración para la microscopía de fluorescencia.

Al Dr. Nicolás Gómez Hernández, mi reconocimiento por su apoyo técnico.

Un especial agradecimiento al LANBAMA por su colaboración y recursos que facilitaron la realización de este estudio.

Agradezco sinceramente a Gloria López por su invaluable ayuda en el laboratorio, la cual fue fundamental para el avance de este proyecto.

A las y los Glabrashians del Laboratorio 6, mi reconocimiento por los conocimientos compartidos, los valiosos consejos y los buenos momentos vividos durante este proceso.

Table of contents

List of Figures

List of Tables

List of Supplementary Figures

List of Supplementary Tables

Abbreviations

OD	Optical density
YPD	Yeast extract-Peptone-Dextrose
YNB	Yeast extract-Nitrogen-Base
YPG	Yeast extract-Peptone-Glycerol
FLC	Fluconazole
FLC^{R}	Fluconazole resistant
FLC^{S}	Fluconazole susceptible
ROS	Reactive oxygen species
SDD	Susceptible dose-dependent
Gly-	Evolved mutant with mitochondrial dysfunction (unable to grow under nonfermentable carbon sources, like glycerol)
Gly+	Evolved mutant with competent mitochondrial respiration (capable of growing under nonfermentable carbon sources, like glycerol)
Pdr1	Transcription factor 1 regulates pleiotropic drug response
ABC	ATP-binding cassette efflux pumps
SET2	Gene coding for Set2, a histone methylase responsible for H3K36
COX2	Gene coding subunit II of the Cytochrome C Oxidase complex
COX3	Gene coding subunit III of the Cytochrome C Oxidase complex
Prx1	Peroxiredoxin 1 mitochondrial protein
GFP	Green fluorescent protein
pP*PGK1*	Promoter for expression of 3-phosphoglycerato kinase (*PGK1*)
NAT	Nourseothricin resistance marker
FRT	Flip1 recombination targets
pP*TEF1*	Promoter for expression of translational elongation factor 1 (*TEF1*)
UTR	Untranslated region
BpM	Base pair marker
bp	Base pair

Resumen

Microevolución de *Candida glabrata* en presencia de fluconazol

Debido a la resistencia a los antifúngicos, las infecciones oportunistas causadas por *C. glabrata* representan riesgos para individuos inmunocomprometidos. Este estudio investiga el papel de la función mitocondrial y la metilación de histonas, particularmente H3K36, en la resistencia a fluconazol (FLC) en *C. glabrata*. Realizamos un experimento de microevolución exponiendo crónicamente tres cepas parentales de *C. glabrata* a FLC, para generar mutantes evolucionadas. Evaluamos la estabilidad del fenotipo de resistencia a FLC (FLC^R) con un ensayo de crecimiento por goteos y construimos un plásmido para la generación de una mutante nula del gen *SET2* (pDC1) para evaluar la metilación de H3K36 en respuesta a FLC. Analizamos la función mitocondrial mediante el crecimiento en fuentes de carbono no fermentables como glicerol (fenotipo Gly-) y realizamos tinciones con MitoTracker™ Green FM y MitoTracker™ Red CMXRos, además de investigar la presencia de los genes mitocondriales *COX2* y *COX3*. También utilizamos una fusión de la proteína mitocondrial Prx1 con GFP para observar la morfología mitocondrial. Nuestros resultados mostraron variabilidad en la estabilidad del fenotipo FLC^R según la cepa. Las mutantes Gly- exhibieron disfunción mitocondrial estable y no revirtieron a Gly+, debido a un posible daño o perdida potencial de los genes *COX2* y *COX3* en algunas cepas. La tinción de las mitocondrias en mutantes Gly- mostró señales de fluorescencia difusa, lo que sugiere alteraciones en la estructura y función mitocondrial. La construcción de pDC1 permitirá estudiar el papel de Set2 en la resistencia a FLC. Estos hallazgos resaltan la compleja relación entre la función mitocondrial y la resistencia a FLC en *C. glabrata*, destacando la necesidad de más investigaciones sobre los mecanismos epigenéticos subyacentes.

Palabras clave: *Candida glabrata*, resistencia a fluconazol, función mitocondrial, fenotipo Gly-, regulación epigenética.

Abstract

Microevolution of *Candida glabrata* in the presence of fluconazole

Due to antifungal resistance, opportunistic infections caused by *Candida glabrata* pose significant health risks to immunocompromised individuals. This study investigates the role of mitochondrial function in fluconazole (FLC) resistance (FLC^R) and the impact of histone methylation, particularly H3K36, in *C. glabrata*. We conducted a microevolution experiment by chronically exposing three *C. glabrata* parental strains to FLC that generated evolved mutants. Using a growth spot assay, we assessed the stability of the FLC^R phenotype. We constructed a knockout plasmid targeting the *SET2* gene (pDC1) to evaluate the role of H3K36 methylation in response to FLC exposure. The mitochondrial function of the evolved mutants was analyzed through growth on non-fermentable carbon sources (Gly- phenotype), by mitochondrial staining with MitoTracker™ Green FM and MitoTracker™ Red CMXRos, and the presence of mitochondrial genes *COX2* and *COX3* was investigated to evaluate mitochondrial structure and function. Also, a translational fusion of the mitochondrial protein Prx1 with GFP was used to observe mitochondrial morphology. Our results showed variability in the stability of the FLC^R phenotype depending on the particular genetic background. Gly- mutants exhibited stable mitochondrial dysfunction and could not revert to Gly+, with potential loss or damage of *COX2* and *COX3* genes. Additionally, Gly- mutants showed diffuse fluorescence signals with mitochondrial stains, suggesting mitochondrial structural and functional alterations compared to Gly+ strains. The Prx1-GFP fusion did not give a fluorescent signal in the Gly- strains, suggesting defects in mitochondrial integrity. Spot growth assays revealed a complex interplay between genetic background, phenotype, and FLC resistance stability. Construction of pDC1 allows the study of the role of Set2 in FLC resistance and its potential reversibility. These findings highlight the intricate relationship between mitochondrial function and FLC^R in *C. glabrata* and the need to further investigate the underlying epigenetic mechanisms.

Keywords: *Candida glabrata*, fluconazole resistance, mitochondrial function, Gly- phenotype, epigenetic regulation

1. Introduction

Opportunistic infections impose significant health risks for individuals with weakened immune systems, as they may rapidly progress and potentially result in increased morbidity and mortality rates. These infections caused by various microorganisms, including viruses, bacteria, parasites, and fungi, exploit the host's weakened defenses (Brown et al. 2012). Their clinical management often proves challenging, as they may resist standard treatments or require more aggressive therapies, further complicating their management (Czura, 2022). The pathogenesis of opportunistic infections typically follows a sequential progression through exposure, adhesion, invasion, and establishment of infection, with the severity of resultant disease manifestations often correlated with the pathogen's virulence (Balloux & van Dorp, 2017). Opportunistic pathogens are known for their phenotypic plasticity, allowing them to alter the expression of different genes in response to changing conditions without affecting their genotype (Czura, 2022).

Candida spp. represent a diverse genus of opportunistic fungi, encompassing over 200 distinct species, with approximately 20% implicated in human infections. While commensally inhabiting the microbiota of healthy individuals, perturbations in microbial equilibrium or compromised immune surveillance can trigger their transition from commensalism to pathogenicity. This transition may lead to candidiasis, a condition resulting from microbial dysbiosis induced by a weakened immune system, disruption of mucosal barriers, or prolonged antibiotic therapy (Brown et al., 2012; Henriques & Williams, 2020). Candidiasis manifests superficially or invasively, with *Candida glabrata* (*C. glabrata*) emerging as a significant etiological agent in both clinical presentations (World Health Organization, 2022).

C. glabrata is an example of an opportunistic pathogenic fungus in humans that can alter the expression of specific genes depending on the environment and enabling it to thrive within its host (Domergue et al., 2005; Juárez-Reyes & Castaño, 2019). Notably, the genetic makeup of *C. glabrata* promotes successful pathogenicity by reducing metabolic function genes and expanding genes related to cell wall organization, which contributes to biofilm formation and adherence properties (Roetzer et al., 2011). While predominantly colonizing human mucosal

linings, recent research by Hassan et al. (2021) suggests environmental reservoirs for *C. glabrata*, expanding the scope of potential infection sources.

According to a recent study conducted by Castanheira et al. (2022) of 561 *C. glabrata* specimens gathered from different parts of the world during 2018-2019 showed that approximately 6.1% of the isolates were resistant to fluconazole (FLC). However, these rates varied by geographical region and were found to be most prevalent in North America (8.1%) followed by Europe (5.9%) (Castanheira et al., 2022). In Mexico, *C. glabrata* ranks as the second most common *Candida* spp. implicated in both superficial and invasive candidiasis, possibly due partly to its inherent lower susceptibility to FLC compared to other *Candida* spp. (Reyes-Montes et al., 2017).

FLC, a member of the azole group of drugs, is typically administered as the first-line therapy for candidiasis. It targets the early biosynthesis stages of ergosterol, an essential constituent of fungal cell membranes, by binding to and inhibiting the lanosterol 14 α-demethylase enzyme. This ultimately leads to damage in the fungal cell membrane and the accumulation of toxic sterols (Healey et al., 2016).

Despite its efficacy, resistance to FLC has emerged in *C. glabrata* through various mechanisms. One of the most prevalent resistant mechanisms involves the overexpression of ATP-binding cassette (ABC) efflux pumps, including Cdr1, Cdr2, and Snq2, which is mediated by mutations in the Cg*PDR1* gene. These mutations increase efflux pumps' expression, allowing *C. glabrata* to expel FLC more efficiently (Gaspar-Cordeiro et al., 2022; Ramage et al., 2002).

In addition to efflux pump overexpression, mitochondrial mutations can contribute to FLC resistance. Alterations in mitochondrial DNA (*COX1, COX2,* and *COX3*) and nuclear DNA coding for proteins involved in mitochondrial function (*MIP1, RDM9, MSY1,* and *CIT1*) disrupt mitochondrial membrane potential and respiration, leading to phenotypically slow-growing “petite” cells. These strains form small colonies and cannot utilize non-fermentable carbon sources such as glycerol, ethanol or acetate and are referred to as Gly-. Although previously considered rare, petite strains have been found in 11% of *C. glabrata* clinical isolates (Borst et al., 2005; Brun et al., 2004; Healey et al., 2016; Siscar-lewin et al., 2021; Helmstetter et al., 2022).

Furthermore, recent studies have shown that mutations in genes encoding for enzymes in charge of histone methylation can also impact FLC resistance in *C. glabrata*. For instance, Baker et al. (2021) reported that the deletion of the Cg*SET1* gene, which encodes for Set1, responsible for histone H3 lysine 4 (H3K4) mono-, di-, and trimethylation, led to an increased susceptibility to azole drugs in both *C. glabrata* and *S. cerevisiae*. In the case of *C. glabrata*, azole induction of many genes involved in ergosterol biosynthesis is controlled epigenetically through the methylation of H3K4 by Set1; therefore, in *set1*Δ mutants, the *ERG* genes are not induced, leading to increased azole susceptibility (Baker et al., 2021).

Moreover, Moirangthem et al. (2021) demonstrated that deletion of the Cg*SET2* gene, which encodes a histone H3 lysine 36 (H3K36) methyltransferase, resulted in moderate resistance to FLC compared to wild-type cells. Bhakt et al. (2022) found that the *C. glabrata set2Δ* mutants exhibited reduced levels of H3K36me3, a histone modification associated with gene transcription when compared to wild-type cells while maintaining normal levels of H3K4me and moderate levels of resistance toward FLC. Altogether, these findings highlight the importance of histone methylation, particularly H3K36me3, in regulating gene expression and FLC resistance in *C. glabrata*.

Further investigations into the molecular mechanisms underlying these epigenetic changes and the alterations in the mitochondrial function may yield valuable insights into the interplay between chromatin remodeling, mitochondrial dynamics, and drug resistance in this pathogenic yeast. By studying how organisms adapt and evolve with microevolution experiments, particularly in response to selective pressures like chronic exposure to antifungal drugs such as FLC, we will begin to understand the relationship between these factors more clearly.

2. Materials and methods

2.1 *C. glabrata* strains

The strains used in this work are described in **Table S 1**.

2.2 Plasmids

The plasmids used in this work are described in **Table S 2**.

2.3 Primers

The primers used in this work are described in **Table S 3**.

2.4 Media

Yeast were grown in standard yeast media as described previously, with 2% agar added to plates (Smith & Burke, 2014). Yeast extract-peptone-dextrose (YPD) medium contains 10 g/L yeast extract and 10 g/L peptone and is supplemented with 2% glucose or glycerol. YPD plates were supplemented with Nourseothricin (Invitrogen™) at 100 µg/mL when required.

Bacteria were grown in LB medium, as described previously (Ausubel et al., 2003). The medium contained 5 g/L yeast extract, 10 g/L tryptone, and 5 g/L NaCl. All plasmid constructs were introduced into strain DH10 by electroporation, and 100 µg/mL carbenicillin (Invitrogen™) was added to select for plasmids. 1.5% agar was used for plates.

2.5 DNA extraction from *C. glabrata*

We employed a rapid DNA extraction method using FastPrep, standardized in our laboratory, to obtain genomic and mitochondrial DNA from yeasts, as described below. We inoculated 5 mL of YPD medium with our strains of interest and incubated them at 30 °C for one overnight with continuous shaking. After incubation, we collected the cells via centrifugation and added 500 µL of buffer A with detergent, followed by an equal volume of phenol:chloroform:isoamyl alcohol. The samples were then subjected to FastPrep (MP Biomedicals) for 1 second at 4 m/s, followed by centrifugation. We added 15 µL of 5M NaCl and 1 mL of cold 100% ethanol to the aqueous phase. The mixture was gently inverted and the DNA pellet was washed

with 1 mL of 70% ethanol. Finally, the samples were resuspended in 250 µL of TE buffer (10 mM Tris, 0.1 mM EDTA, pH 8). Subsequently, 0.2 µL of an RNAse cocktail was added to each sample.

2.6 Plasmid DNA extraction from *Escherichia coli*

To extract plasmids contained in E. coli DH10 cells, we employed the Zippy Plasmid Miniprep commercial kit (Zymo Research).

2.7 Yeast transformation

Yeast transformations with digested or supercoiled plasmids were performed as previously described using the LiOAc/salmon sperm carrier ssDNA/PEG method (Smith & Burke, 2014).

2.8 Microevolution experiment to study acquired FLC resistance in *C. glabrata*

Our laboratory previously conducted a microevolution experiment involving three *C. glabrata* parental strains, including two clinical isolates (one resistant and one susceptible to FLC) and the BG14 standard strain. We exposed these strains to chronic FLC exposure at concentrations ranging from 8 to 256 µg/mL, reinoculating strains every day to fresh media at the same FLC concentration for 15 days, followed by three passes in YPD medium without FLC and an additional six passes. After the nine passes, we isolated two types of FLC resistant mutants (FLC^R) referred to as "evolved mutants": those that were unable to grow in glycerol (Gly-) as a carbon source and, therefore, unable to respire and have dysfunctional mitochondria, and those that were able to grow in glycerol (Gly+) and thus respiration competent cells (**Figure S 1)**.

2.9 Characterization of *C. glabrata* evolved mutants from microevolution experiment

2.9.1 Purification of colonies obtained from five and ten days in FLC and nine subcultures in YPD with a Gly+ and Gly- phenotype

After chronic exposure to FLC, samples were collected from cultures on days five and ten and grown at different FLC concentrations for the reference strain BG14 and the two clinical isolates of *C. glabrata*. The selected colonies were subsequently plated in YPD agar plates, and two colonies from each strain and time point were isolated and straked for pure colony isolation. Furthermore, strains derived from the three subcultures in YPD were subjected to six additional passes in YPD medium and subsequently purified.

Respiratory function was assessed using a growth assay on a solid medium with glycerol, a non-fermentable substrate, as the sole carbon source. Colonies demonstrating deficient respiratory function referred to as the Gly- phenotype, or competent respiratory function, known as the Gly+ phenotype, were stored in 15% glycerol at -70°C for future analyses. This storage included colonies from different stages of the evolution experiment (days five and ten under FLC exposure and nine accumulated subcultures in YPD).

2.9.2 Analysis for reversion of the Gly- to Gly+ phenotype in evolved mutants

We investigated whether the evolved Gly- mutants can revert to the Gly+ phenotype to analyze possible adaptation mechanisms and FLC resistance development in *C. glabrata*.

We took samples of our evolved Gly- mutants derived from the three parental strains and grew them in liquid YPD medium to a saturated OD. Then, we inoculated 10 µL of each sample into tubes containing liquid YPG medium, and a tube with fresh YPD medium was used as a positive control. We incubated the tubes with YPG at 28°C in a roller for five overnights (the positive controls were incubated for one overnight). We plated 100 µL of each saturated culture from the positive control on Petri dishes containing YPG and incubated them for four overnights at 30 °C, see **Figure S 2**.

2.9.3 Amplification of *COX2* and *COX3* genes in Gly- evolved mutants by endpoint PCR

We analyzed whether the lack of reversibility of the Gly- to the Gly+ phenotype in these evolved mutants could be related to the loss of fragments of mitochondrial DNA (mtDNA); we determined the presence of two mitochondrially encoded genes,

COX2 and *COX3*, by end-point PCR. Given the key role of mitochondria in cellular respiration and energy production, any mutations within the mtDNA could impact mitochondrial function, thereby influencing the respiratory capacity of the evolved mutants.

We used two sets of primers (see **Table S 3**) to identify possible deletions in the mitochondrial DNA by endpoint PCR. These primers amplify a region of 121 bp and 124 bp, respectively, of the genes encoding subunits II and III of the Cytochrome C Oxidase (COX) complexes (*COX2* and *COX3,* respectively), which are essential components of the mitochondrial electron transport chain (Lipinski et al., 2010).

2.9.4 Analysis of mitochondrial structure

We decided to analyze the structure of the mitochondria in the evolved mutants to determine if there are differences between the mitochondrial structures of the Gly- and Gly+ evolved mutants compared to their respective parental strains.

2.9.4.1 Analysis of mitochondrial morphology assessed by MitoTracker™ green FM staining

To examine the morphology of mitochondria in our evolved mutants, we used MitoTracker™ Green FM by Invitrogen™ 7514 in combination with fluorescence microscopy. This fluorescent dye is designed to stain mitochondria in live cells independently of the mitochondrial membrane potential by binding to mitochondrial proteins, such as Cytochrome C, and accumulating inside the mitochondria. The staining intensity of MitoTracker™ Green FM is directly proportional to the mitochondrial mass of the cells (Thermo Scientific, 2023).

To stain and observe mitochondria, overnight cultures of each strain were reinoculated in 5 mL of YNB+uracil medium at an OD_{600} of 1.5 and incubated in a roller at 30°C for 2 hours. 1 mL of each culture was transferred to 1.5 mL Eppendorf tubes, and cells were washed once with sterile water. finally, the cells were resuspended in 200 µL of 1X stock of MitoTracker™ green FM and incubated for 30 minutes before observation under a fluorescence microscope Zeiss Axio Vision Blue edition.

2.9.4.2 Assess mitochondrial integrity

We decided to assess the integrity of the inner mitochondrial membrane in both the Gly+ and Gly- evolved mutants by tagging with GFP the Prx1 protein (a peroxiredoxin-1), a protein localized in the inner membrane of the mitochondria (Gomes et al., 2017). Changes in Prx1 localization or expression patterns suggest alterations in this membrane.

We transformed the parental Gly+ strains, the evolved mutants from day 15 in FLC, those from three subcultures in YPD, and the CGM1938 using the plasmid pFA1 (see **Table S 2**). This plasmid contains a translational fusion of Prx1, a peroxiredoxin involved in cellular redox homeostasis, with GFP and driven by the *PGK1* gene promoter for high constitutive expression of Prx1-GFP.

2.9.4.3 Analysis of mitochondria assessed by MitoTracker™ Red CMXRos 7513

We employed Mitotracker™ Red CMXRos 7513, a cationic dye with a high affinity for active mitochondria. This dye accumulates within these organelles based on the production of reactive oxygen species (ROS) (Thermo Scientific, 2023). Mitochondria are the main generators of ROS, as a byproduct of oxidative phosphorylation, a process that occurs in the inner mitochondrial membrane (Okamoto et al., 2023). Therefore, staining cells with Mitotracker™ Red CMXRos serves as a visual marker to assess mitochondrial functionality.

Cells were grown and treated as described for MitoTracker™ Green FM, but in the last step, cells were resuspended in 200 µL of 1X stock of Mitotracker™ Red CMXRos and thoroughly mixed. Finally, the Mitotracker was incubated for 30 minutes before observation under Zeiss Axio Vision Blue edition microscope.

2.9.5 Spot growth assay to evaluate the stability of FLC^R phenotype

We conducted a spot growth assay, in which the evolved mutants from each genealogy of the BG14 (standard laboratory strain), AN378 (FLC^R clinical isolate), and AN755 (FLC^S clinical isolate) were cultured in YPD medium to stationary phase, and the cell density was adjusted to an optical density (OD_{600}) of 1. We also included two control strains, one susceptible, *pdr1*Δ, and one resistant, *hst1*Δ, to FLC. Dilutions of the cell culture were prepared at ratios of 1:0 (undiluted), 1:10, 1:100, 1:1000, and 1:10000 using sterile milliQ water. Using a replicator of 6x8 pins, we

spotted each cell suspension on YPD+FLC agar plates containing different concentrations of FLC [0, 32, 64, and 128 μg/mL]. After incubation at 30°C for 48 hours, the plates were photographed. The growth patterns were analyzed to determine the susceptibility of each evolved mutant to FLC, considering the size and density of the spots at each dilution and fluconazole concentration. The assay was repeated three times to evaluate reproducibility.

3. Results

3.1 Microevolution experiment demonstrates that chronic exposure of *C. glabrata* strains to FLC results in the development of fluconazole-resistant evolved mutants

To study the development of resistance and adaptation to FLC of three different *C. glabrata* strains, including the laboratory standard (BG14) and two clinical isolates (one previously determined to be resistant and one sensitive to FLC), we conducted a microevolution experiment in the presence of FLC (see **Figure S 1**). We continuously cultivated these strains with chronic FLC exposure at concentrations ranging from 8 to 256 µg/mL for 15 days with the corresponding FLC concentration. We purified colonies from different concentrations of FLC for further characterization. To determine the stability of the acquired resistance to FLC, we subcultivated the strains isolated after 15 days of FLC exposure for three continuous passes in YPD medium without FLC and then an additional six passes for a total of nine passes without FLC.

After the nine passes in the absence of FLC, we isolated two types of FLC resistant (FLC^R) mutants referred to as “evolved mutants”: 1) those that were unable to grow in glycerol (Gly-) as a carbon source as a result of having dysfunctional mitochondria (unable to respire), and 2) those that were able to grow in glycerol (Gly+) and thus respiration competent cells.

The microevolution experiment demonstrates that exposing *C. glabrata* strains to chronic FLC results in the development of fluconazole-resistant evolved mutants. These exhibit distinct characteristics regarding their ability to grow in glycerol as a carbon source, indicating variations in mitochondrial function. The emergence of both Gly+ and Gly- evolved mutants suggests a complex interplay between mitochondrial function and FLC resistance in *C. glabrata*, see **Figure S 2**.

3.2 Mitochondrial dysfunction in evolved Gly- mutants does not revert and enhances FLC resistance in *Candida glabrata*

We next decided to investigate whether the evolved Gly- mutants can revert to the Gly+ phenotype to analyze possible adaptation mechanisms and FLC resistance development in *C. glabrata*.

We took samples of our evolved Gly- mutants from the three strains and grew them in liquid YPD medium to a saturated OD. Then, we inoculated 10 µL of each sample into tubes containing liquid YPG medium and a tube with fresh YPD medium used as a positive control. We incubated the tubes with YPG at 28°C in a roller for five overnights (the positive controls were incubated for one overnight). We plated 100 µL of each saturated culture from the positive controls on petri dishes containing YPG and incubated them for four overnights at 30 °C.

None of the cultures grew in liquid YPG medium after five overnights, and none of the cells from the YPD overnight grew when plated on YPG (see **Figure 1**).

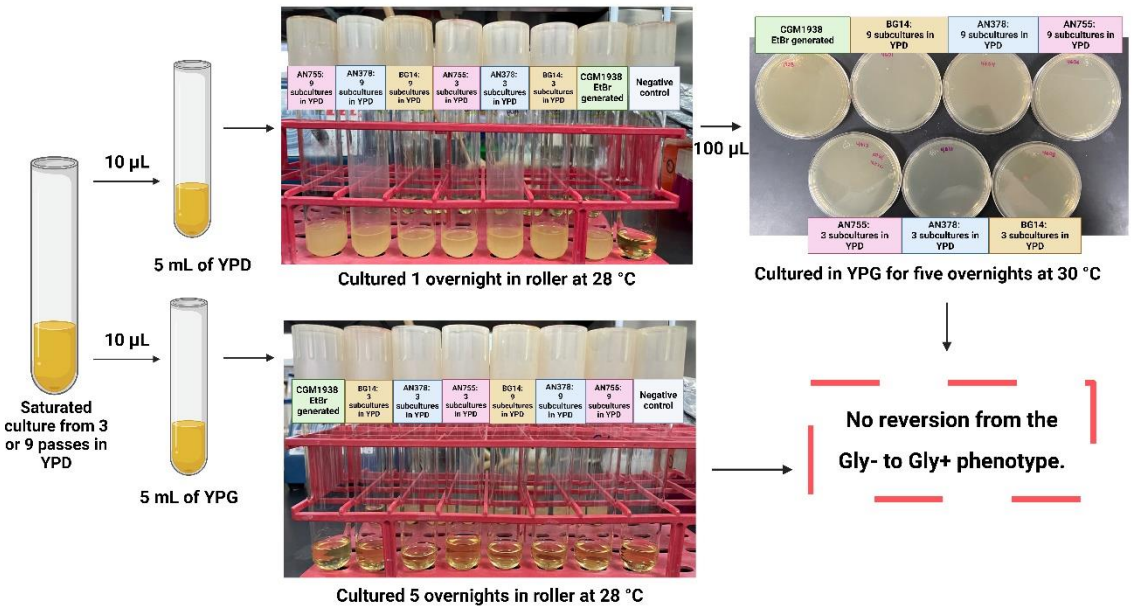

Figure 1. Schematic representation of the experiment designed to study reversion from the Gly- to the Gly+ phenotype.

285

The absence of growth in liquid YPG medium and on YPG plates indicates the inability of these mutants to switch back to a phenotype with functional mitochondria. These findings suggest that once the parental strains develop resistance to FLC through the generation of mitochondria defective mutants (Gly-), this phenotype persists.

We analyzed whether the lack of reversibility of the Gly- to the Gly+ phenotype in these evolved mutants could be related to the loss of fragments of mtDNA. We determined the presence of two mitochondrially encoded genes, *COX2* and *COX3*, by end-point PCR.

3.3 Variations in *COX2* and *COX3* gene amplification indicate potential mitochondrial alterations in Gly- evolved mutants

Given the key role of mitochondria in cellular respiration and energy production, any mutations within the mtDNA could impact mitochondrial function, thereby influencing the respiratory capacity of the evolved mutants.

We used two sets of primers (see **Table S 3**) to identify possible deletions in the mitochondrial DNA by endpoint PCR. These primers amplify a region of 121 bp and 124 bp, respectively, of genes coding subunits of the Cytochrome C Oxidase (COX) complexes II and III (*COX2* and *COX3,* respectively), which are essential components of the mitochondrial electron transport chain (Lipinski et al., 2010). All evolved mutant DNA was diluted to a final concentration of 10 ng/µL for PCR to ensure consistent DNA concentration across samples.

The results revealed variations in the intensity of amplified bands for *COX2* and *COX3* genes across different genealogies, as shown in **Figure 2**. In the BG14 genealogy, the parental Gly+ strain exhibited higher band intensity for both genes than Gly- mutants. In the AN378 (FLC^R) genealogy, the Gly+ parental strain showed a high band intensity, while the rest of the genealogy displayed undetectable band intensity, except for the strain exposed to FLC for five days, which showed a faint band. For the AN755 (FLC^S) genealogy, differences in band intensity were observed based on the region of the amplified gene. The *COX2* band intensity was consistent across strains, while *COX3* band intensity varied across exposure times, with decreased intensity seen in longer FLC exposures and subcultures in YPD. The

strain generated with EtBr, used as a Gly- control, displayed similar band intensity for both the parental and the strain subcultured in the absence of FLC. However, we could not conclusively determine the absence of amplified products in strains lacking bands, as the negative control without DNA also showed a band of the same size as our amplified product.

322

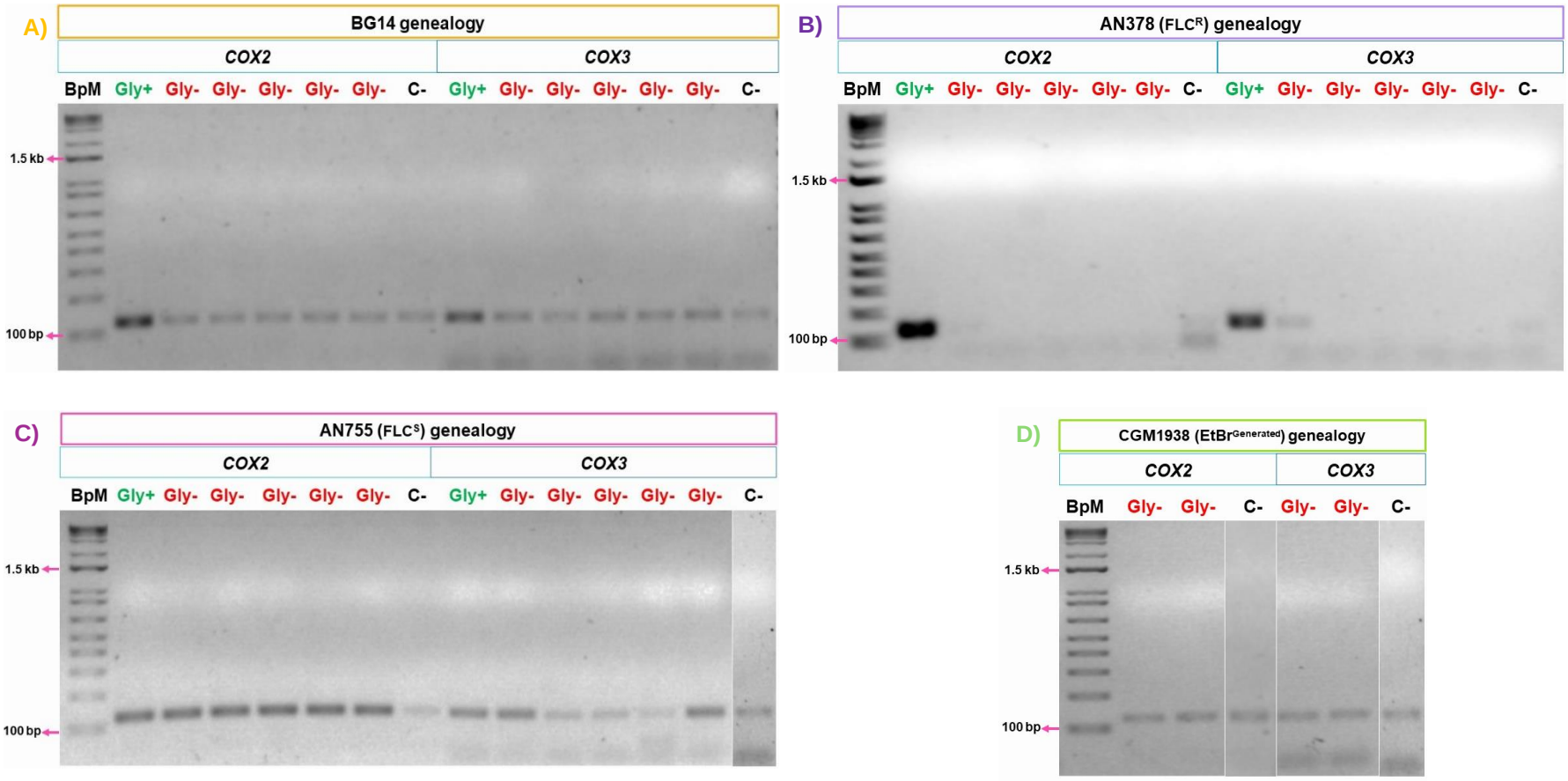

Figure 2. Agarose gel of PCR products of COX2 and COX3 mitochondrial genes.
The order of the lanes for the genealogies on A, B, and C on the gel is parental strain, day five, 10, and 15 in FLC, and three and nine subcultures in YPD. The order of the lanes on D on the gel is parental strain and six subcultures in YPD. For negative control (C-), sterile Mili-Q water was used.

Notably, the differences in band intensity observed in the *COX2* and *COX3* gene amplification could imply variations in the amount of mtDNA relative to nuclear DNA in the Gly- mutants, potentially contributing to their impaired respiratory capacity. Hence, to obtain more precise results, future experiments will focus on studying the ratio of mitochondrial to nuclear DNA in Gly- compared to Gly+ evolved mutants using qPCR with *COX2* and *COX3* mitochondrial gene primers and a single copy nuclear gene (*CYT1*) (primer details in **Table S 3**).

We then analyzed the structure of the mitochondria in our evolved mutants to determine if there are differences between the mitochondrial structures of the Gly- and Gly+ evolved mutants compared to their respective parental strains.

3.4 Gly- evolved mutants have different mitochondrial morphology than Gly+ counterparts assessed by MitoTracker™ green FM staining

To examine the morphology of mitochondria in our evolved mutants, we employed MitoTracker™ Green FM by Invitrogen™ 7514 in combination with fluorescence microscopy. This fluorescent dye is designed to stain mitochondria in live cells independently of the mitochondrial membrane potential by binding to mitochondrial proteins, such as Cytochrome C, and accumulating inside the mitochondria. The staining intensity of MitoTracker™ Green FM is directly proportional to the mitochondrial mass of the cells (Thermo Scientific, 2023).

To observe mitochondria, overnight cultures of each strain were reinoculated in 5 mL of YNB+uracil medium at an OD_{600} of 1.5 and incubated in a roller at 30°C for 2 hours. 1 mL of each culture was transferred to 1.5 mL Eppendorf tubes, and cells were washed once with sterile water. Finally, the cells were resuspended in 200 µL of 1X stock of MitoTracker™ green FM (final concentration of 100 µM) and incubated for 30 minutes before observation under a fluorescence microscope Zeiss Axio Vision Blue edition.

We observed that all the Gly+ and Gly- strains from days 0 and 15 in FLC and three and nine subcultures in YPD have visible mitochondria. However, there is a significant difference between the parental Gly+ strains, which have a well-defined

353 mitochondrial matrix and a more localized fluorescence pattern, compared to the
354 Gly- mutants, which have a more diffuse fluorescent signal (see **Figure 3**).
355

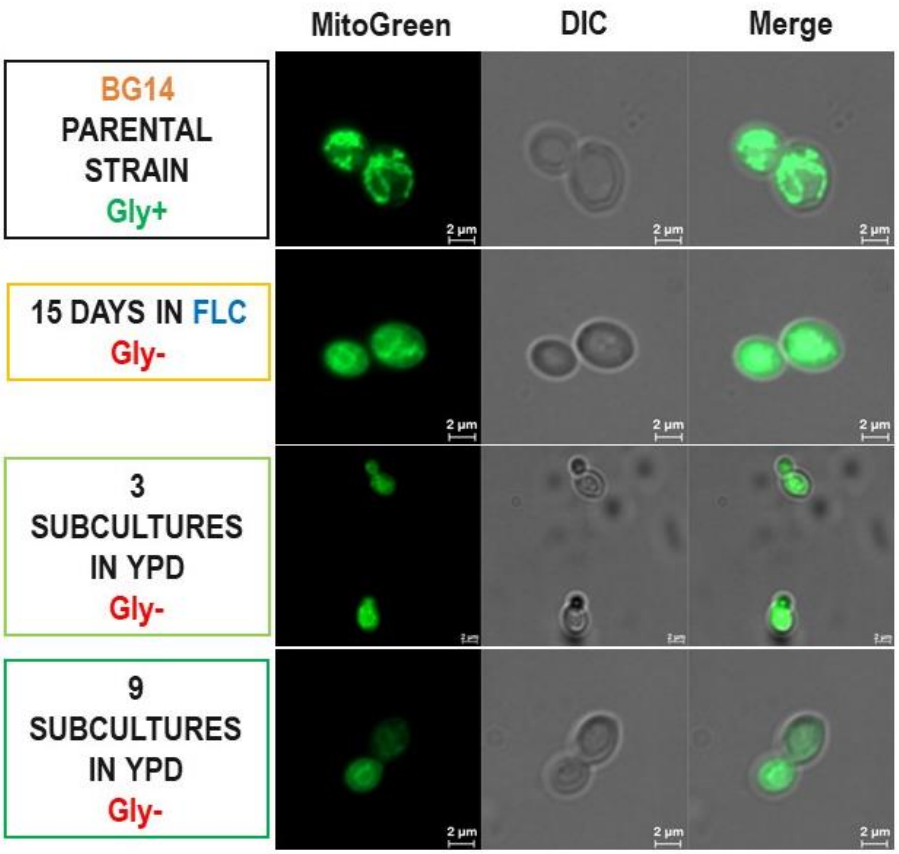
MitoGreen
DIC
Merge
BG14
PARENTAL
STRAIN
Gly+
15 DAYS IN FLC
Gly-
3
SUBCULTURES
IN YPD
Gly-
9
SUBCULTURES
IN YPD
Gly-
2 µm

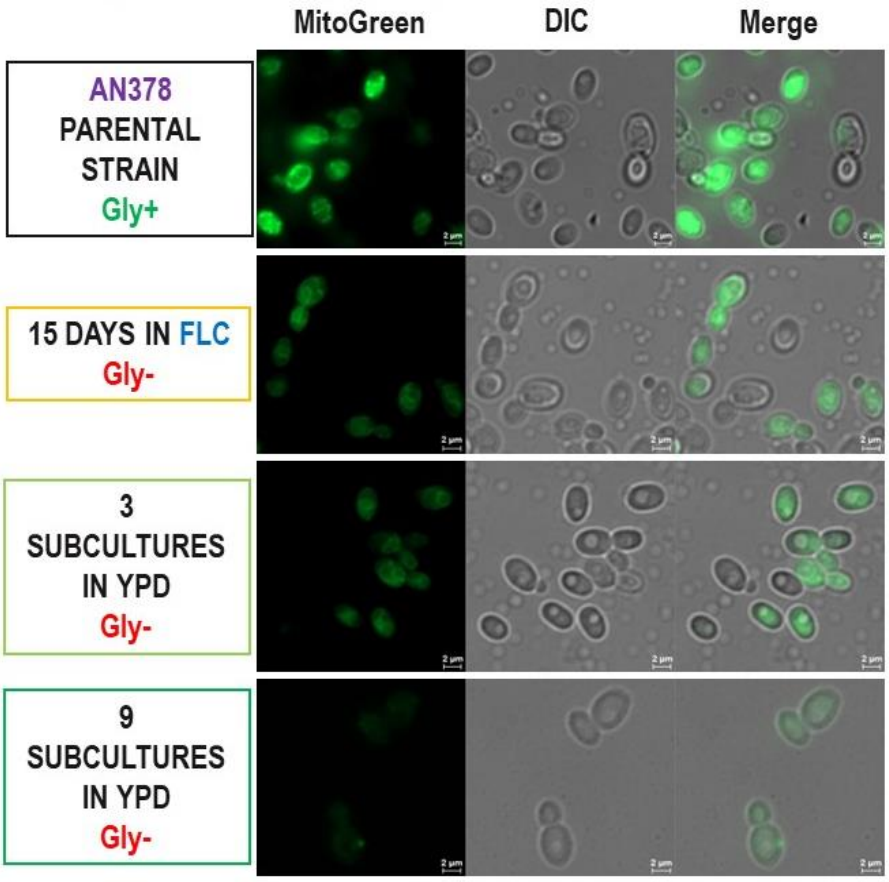
MitoGreen
DIC
Merge
AN378
PARENTAL
STRAIN
Gly+
15 DAYS IN FLC
Gly-
3
SUBCULTURES
IN YPD
Gly-
9
SUBCULTURES
IN YPD
Gly-
2 µm

356

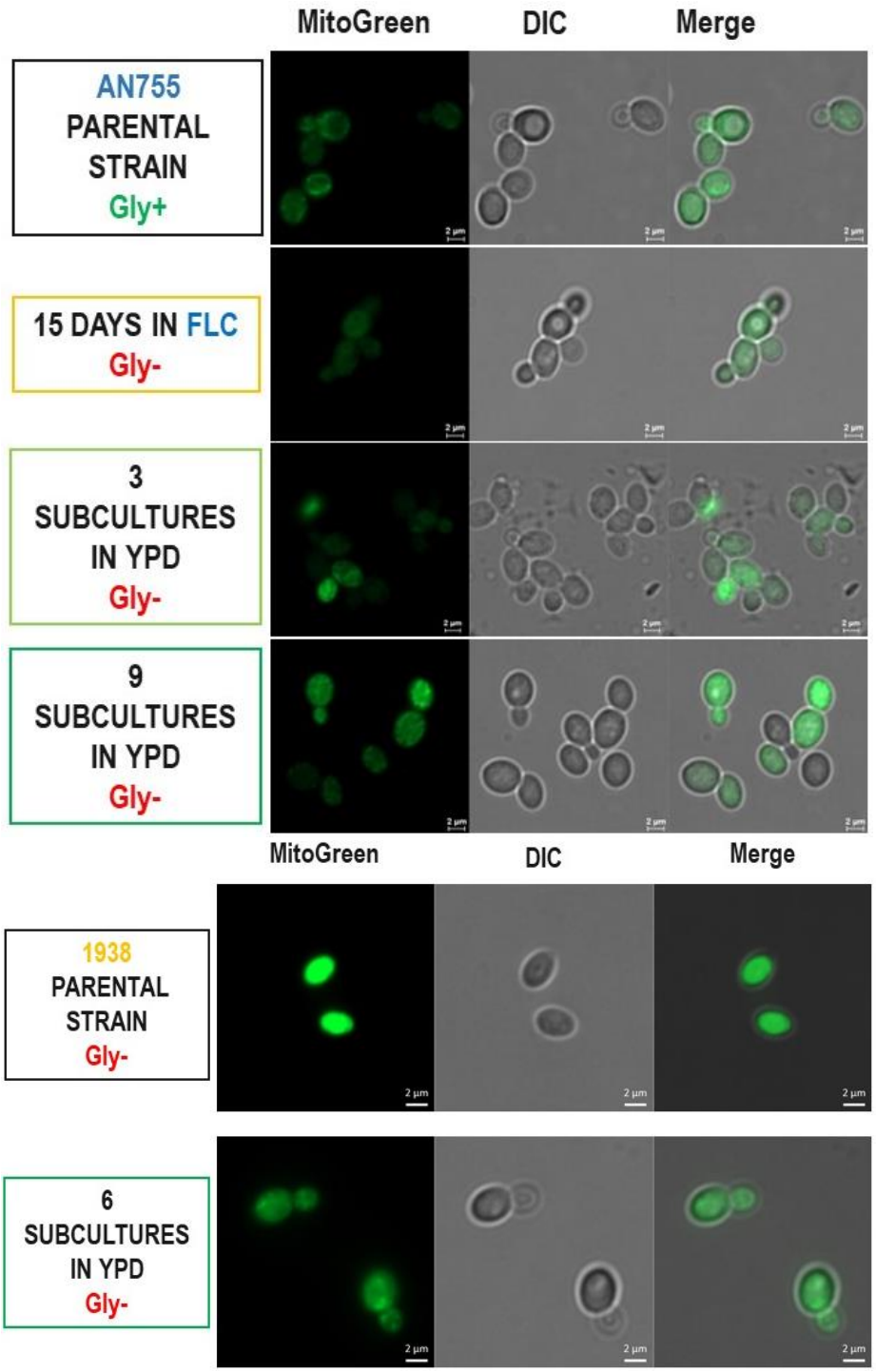

Figure 3. Micrographs with MitoTracker™ green FM of C. glabrata evolved mutants.

We show the staining of mitochondria in the three parental strains and their respective evolved mutants from day 15 in FLC and three and nine subcultures in YPD.

The observed differences in mitochondrial morphology with MitoTracker™ Green FM between the parental Gly+ strains and the Gly- evolved mutants suggest alterations in mitochondrial structure, organization, and function.

We decided to observe and assess the integrity of the mitochondrial matrix in both the Gly+ and Gly- evolved mutants by tagging with GFP the Prx1, a peroxiredoxin-1 involved in cellular redox homeostasis, localized in the inner membrane of the mitochondria.

3.5 Gly- evolved mutants do not contain Prx1-GFP staining

Changes in Prx1 localization or expression patterns may indicate alterations in the inner mitochondria membrane.

We transformed the parental Gly+ strains, the evolved mutants from day 15 in FLC, those from three subcultures in YPD, and the CGM1938 (a Gly- strain obtained after exposure to ethidium bromide) using the plasmid pFA1. This plasmid contains a translational fusion at the C-terminal end of Prx1 with GFP. The P_{PGK1} promoter controls the expression of Prx1-GFP for high constitutive expression.

The analysis under the microscope of the transformed Gly+ evolved mutants containing the pFA1 plasmid revealed distinct and localized fluorescence in the mitochondria in the parental strains compared to the Gly- evolved mutants from 15 days in FLC, and the three subcultures in YPD, that did not exhibit any fluorescence (see **Figure 4**).

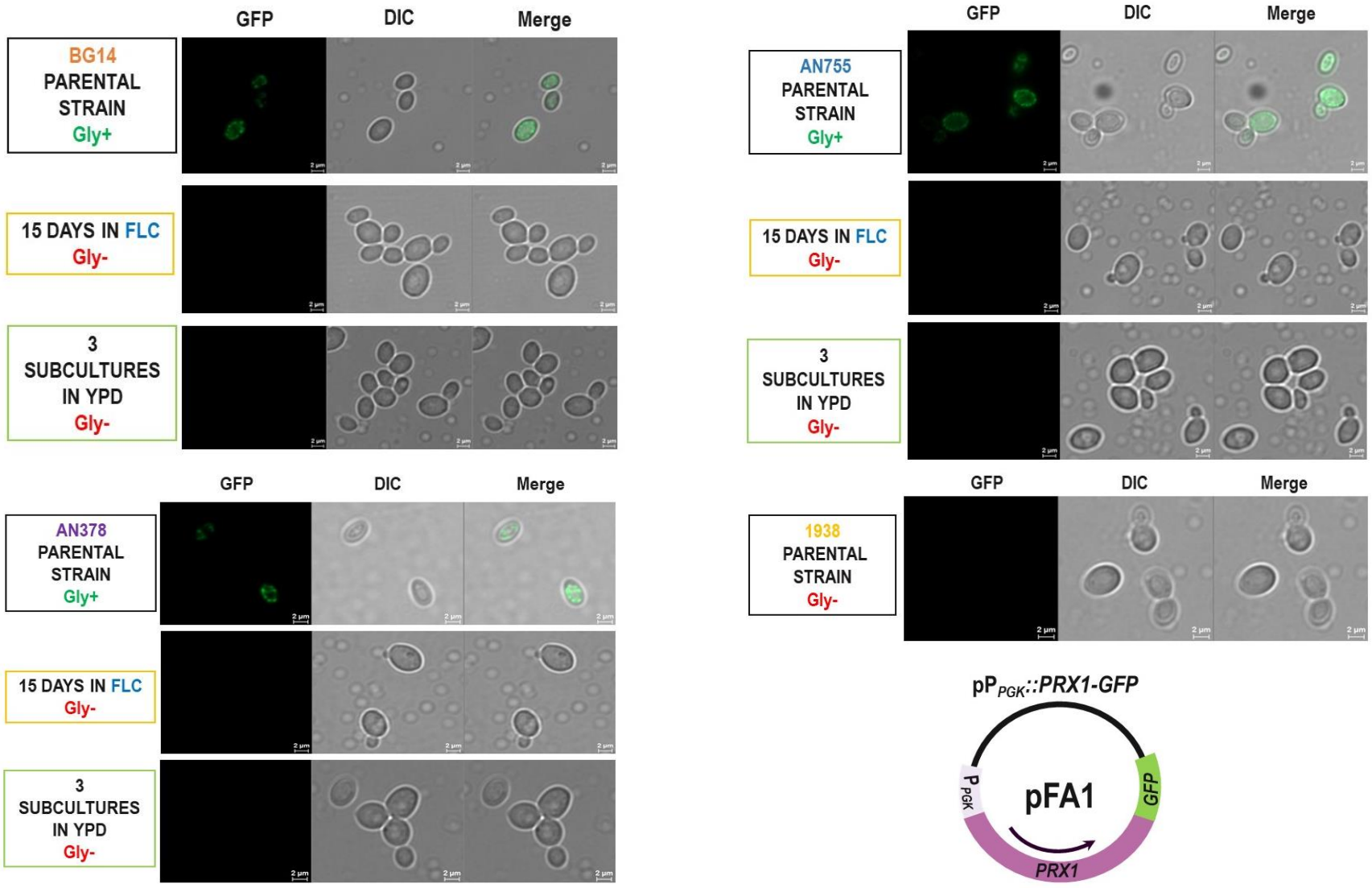

381 ***Figure 4. Micrographs of the parental strains and the corresponding Gly- evolved mutants (grown for 15 days with FLC and three subcultures in YPD without FLC) transformed with plasmid pFA1.***

The differences in Prx1-GFP localization patterns between Gly+ and Gly- evolved mutants after exposure to FLC provide insights into the impact of FLC exposure on mitochondrial health. These findings suggest chronic FLC exposure can cause defects in mitochondrial function, leading to an acquired FLC resistance.

Since Gly- evolved mutants contain mitochondria with morphological alterations as judged by MitoTracker™ Green FM, we next studied mitochondrial function in the Gly+ and Gly- evolved mutants with Mitotracker™ Red CMXRos 7513, a dye for which the fluorescent properties are modulated by the redox environment and metabolic state of mitochondria.

3.6 Mitotracker™ Red CMXRos reveals differences in mitochondrial functionality between Gly+ and Gly- evolved mutants

We employed Mitotracker™ Red CMXRos, a reduced cationic dye that fluoresces upon oxidation (Thermo Scientific, 2023). Since ROS are a byproduct of oxidative phosphorylation, cells with dysfunctional mitochondria have been shown to accumulate these potent signaling molecules (Okamoto et al., 2023). Therefore, staining cells with Mitotracker™ Red CMXRos serves as a visual marker to assess mitochondrial functionality.

Cells were grown and treated as described for MitoTracker™ Green FM, but in the last step, cells were resuspended in 200 µL of 1X stock of Mitotracker™ Red CMXRos (final concentration of 0.5 µM) and thoroughly mixed. Finally, the Mitotracker was incubated for 30 minutes before observation under a microscope.

With Mitotracker™ Red CMXRos, we observed notable differences among the three genealogies. Specifically, the AN755 (FLC^S) genealogy displayed enhanced uptake and diffusion of the dye within the mitochondrial matrix compared to the BG14 and AN378 (FLC^R) genealogies, where the dye displayed more diffuse staining throughout the entire cell. Furthermore, parental strains (with a Gly+ phenotype) demonstrated a distinct mitochondrial matrix with a localized fluorescence pattern, contrasting with Gly- strains from days 15 in FLC and three and nine subcultures in YPD in which diffuse fluorescence was observed. These variations in staining patterns suggest differences in mitochondrial function between

412 Gly+ and Gly- phenotypes, correlating with proper mitochondrial functionality in the
413 Gly+ phenotype (see **Figure 5**).

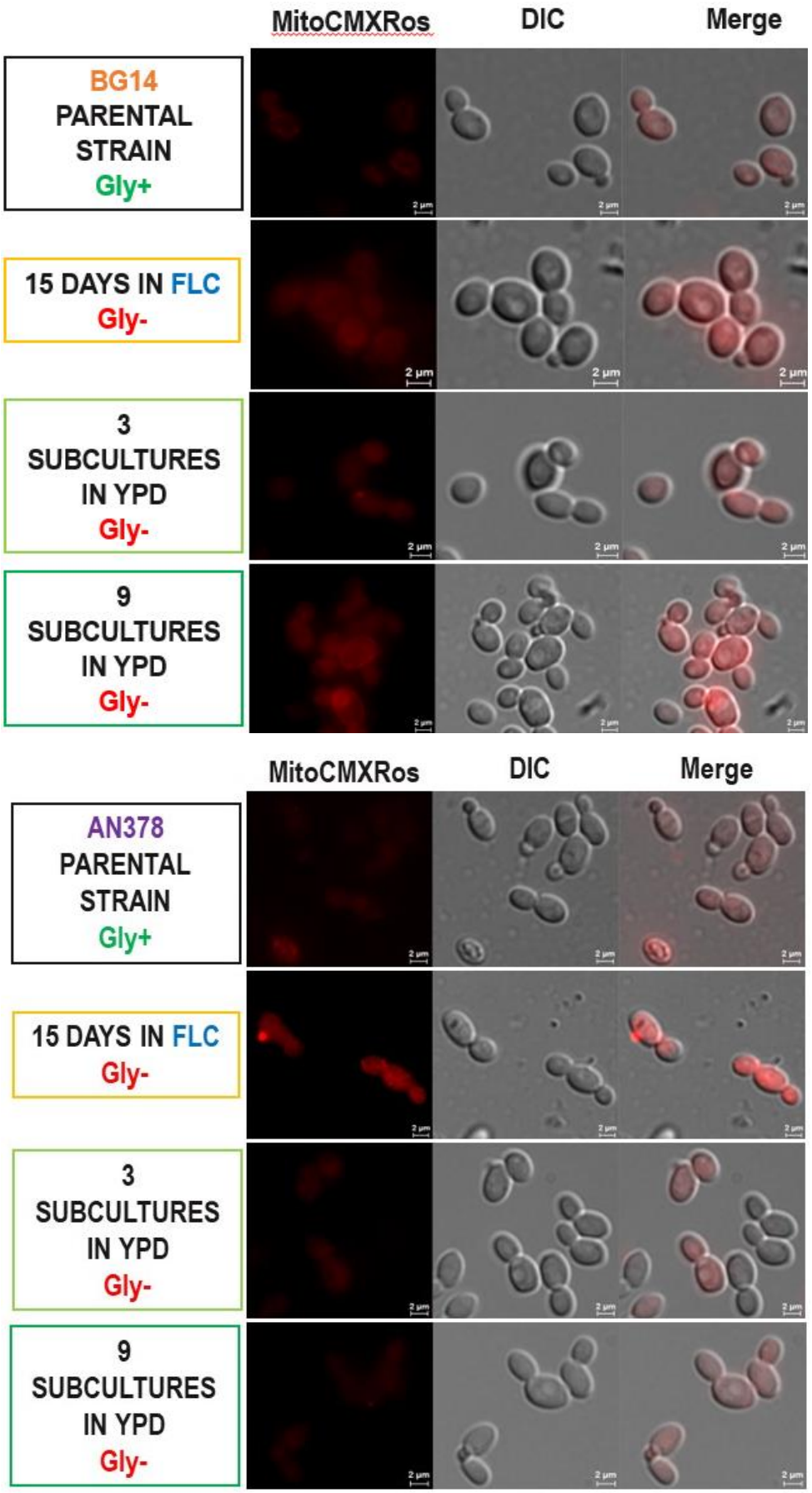
MitoCMXRos
DIC
Merge
BG14
PARENTAL
STRAIN
Gly+
15 DAYS IN FLC
Gly-
3
SUBCULTURES
IN YPD
Gly-
9
SUBCULTURES
IN YPD
Gly-
MitoCMXRos
DIC
Merge
AN378
PARENTAL
STRAIN
Gly+
15 DAYS IN FLC
Gly-
3
SUBCULTURES
IN YPD
Gly-
9
SUBCULTURES
IN YPD
Gly-

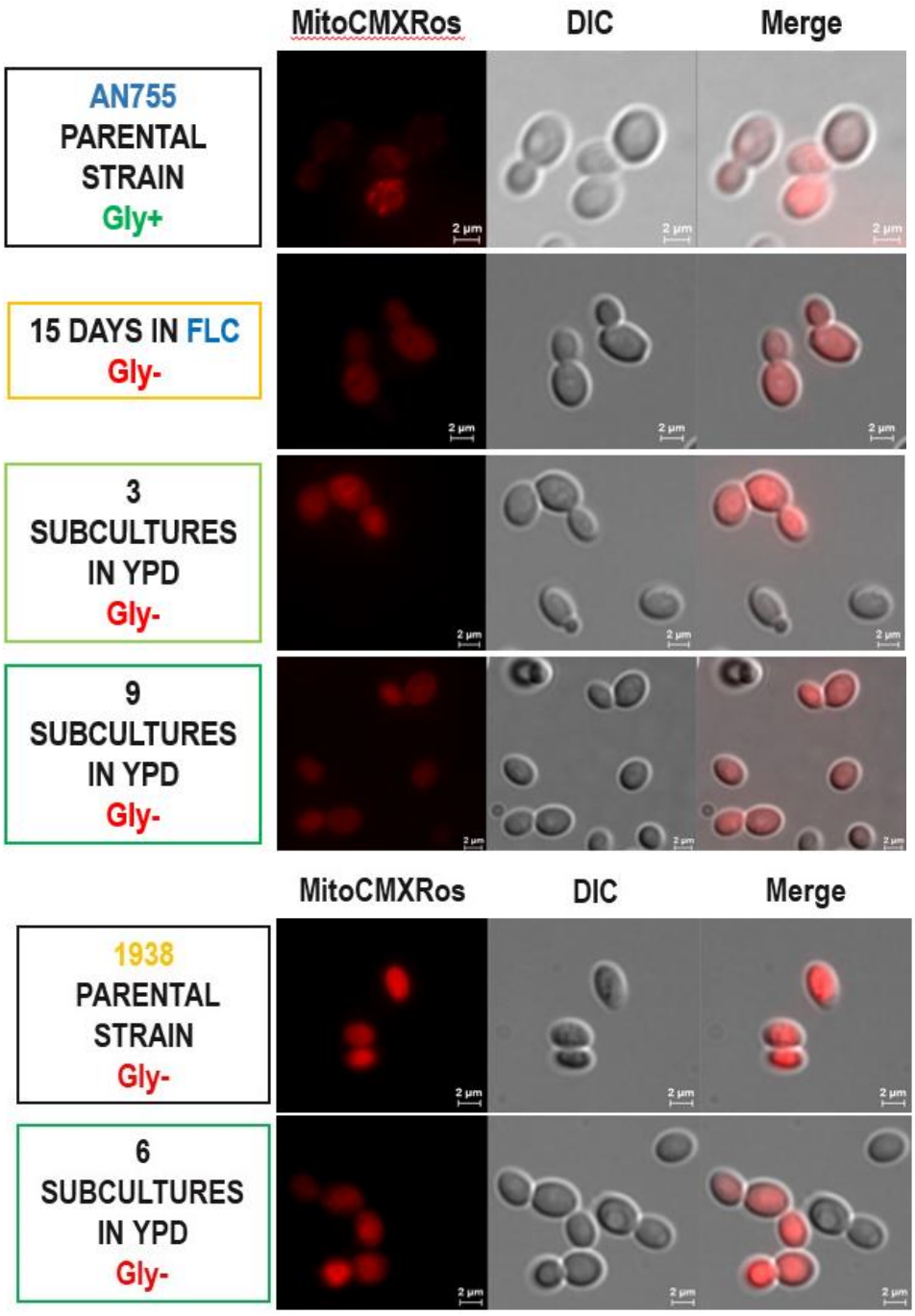

Figure 5. Micrographs with MitoTracker™ Red CMXRos of evolved mutants.

Mitochondria staining of the three parental strains and their corresponding evolved mutants from day 15 in FLC and three and nine accumulated subcultures in YPD.

The use of Mitotracker™ Red CMXRos staining in both Gly+ and Gly- evolved mutants suggests the presence of ROS in the mitochondria of these cells, and probably also, there is ROS not constrained to the mitochondrial compartment in the Gly- evolved strains that are stained with this dye.

We next aimed to characterize the stability of the FLC^R phenotype in the selected Gly+ and Gly- evolved mutants by subculturing the evolved strains from the three genealogies in rich media in the absence of FLC (three or nine subcultures).

3.7 Spot growth assay demonstrates differential stability of fluconazole resistance in Gly- and Gly+ evolved mutants

We conducted a spot growth assay, in which the evolved mutants from each genealogy [BG14 (standard laboratory strain), AN378 (FLC^R clinical isolate), and AN755 (FLC^S clinical isolate)] were cultured in YPD medium to stationary phase, and the cell density was adjusted to an optical density (OD_{600}) of 1. We also included two control strains, one susceptible, *pdr1*Δ, and one resistant, *hst1*Δ, to FLC. Serial 10-fold dilutions of each cell culture were prepared from 10^0 to 10^{-5} in sterile milliQ water. Using a replicator of 6x8 pins we spotted each cell suspension onto YPD agar plates containing different concentrations of FLC [0, 32, 64 and 128 µg/mL]. After incubation at 30°C for 48 hours, the plates were photographed. The growth patterns were analyzed considering the size and density of the spots at each dilution and fluconazole concentration. The assay was repeated thrice to evaluate reproducibility (see **Figure 6**).

In **A,** we show the genealogy of the Gly- and Gly+ evolved mutants derived from the standard laboratory strain BG14. We found that the evolved mutants with a Gly- and Gly+ phenotype have a stable FLC^R phenotype even after nine total subcultures without FLC. However, in the Gly+ evolved mutants, the level of FLC resistance is similar to that of its parental strain.

In **B,** we present the genealogy of the Gly- and Gly+ evolved mutants derived from the FLC^R clinical isolate AN378. The Gly- evolved mutants show an unstable acquired resistance phenotype (FLC concentration of 128 µg/mL). On the other hand, the evolved mutants with a Gly+ phenotype exhibit a stable resistance phenotype like their parental strain.

In **C, we** show the genealogy of the Gly- and Gly+ evolved mutants from the FLC^S clinical isolate AN755. We found that the mutants with a Gly- phenotype have an unstable resistance phenotype in the strains from the subcultures in YPD. They became almost as sensitive as their parental strain. However, the mutants with a Gly+ phenotype showed a stable acquired resistance.

Finally, **D** shows the genealogy of a petite mutant generated with ethidium bromide (EtBr) in the background of the standard strain BG14. This mutant may have multiple mutations, as EtBr acts as a DNA intercalant. We found that this mutant shows an unstable acquired resistance to FLC. In **Table 1**, we summarize the obtained results of the spot growth assay in the presence of FLC by genealogy.

460 **Table 1. Summary of acquired FLC resistance of evolved mutants by genealogy**

Evolved time	Gly phenotype	Acquired FLC^{R}
BG14 genealogy		
Day 0 in FLC	+	S
Day 5 in FLC	+	S
	-	S
Day 10 in FLC	+	US
	-	S
Day 15 in FLC	+	S
	-	S
Three subcultures in YPD	+	S
	-	S
Nine subcultures in YPD	+	S
	-	S
AN378 FLC^{R} genealogy		
Day 0 in FLC	+	S
Day 5 in FLC	+	S
	-	S
Day 10 in FLC	+	S
	-	S
Day 15 in FLC	+	S
	-	US
Three subcultures in YPD	+	S
	-	US
Nine subcultures in YPD	+	S
	-	US
AN755 FLC^{S} genealogy		
Day 0 in FLC	+	S
Day 5 in FLC	+	S

	-	**US**
Day 10 in FLC	**+**	**S**
	-	**US**
Day 15 in FLC	**+**	**S**
	-	**US**
Three subcultures in YPD	**+**	**S**
	-	**US**
Nine subcultures in YPD	**+**	**S**
	-	**US**
CGM1938 generated with EtBr genealogy		
Day 0 in FLC	-	**S**
Six subcultures in YPD	-	**US**

461 US, unstable FLC resistance, and S, stable FLC resistance.

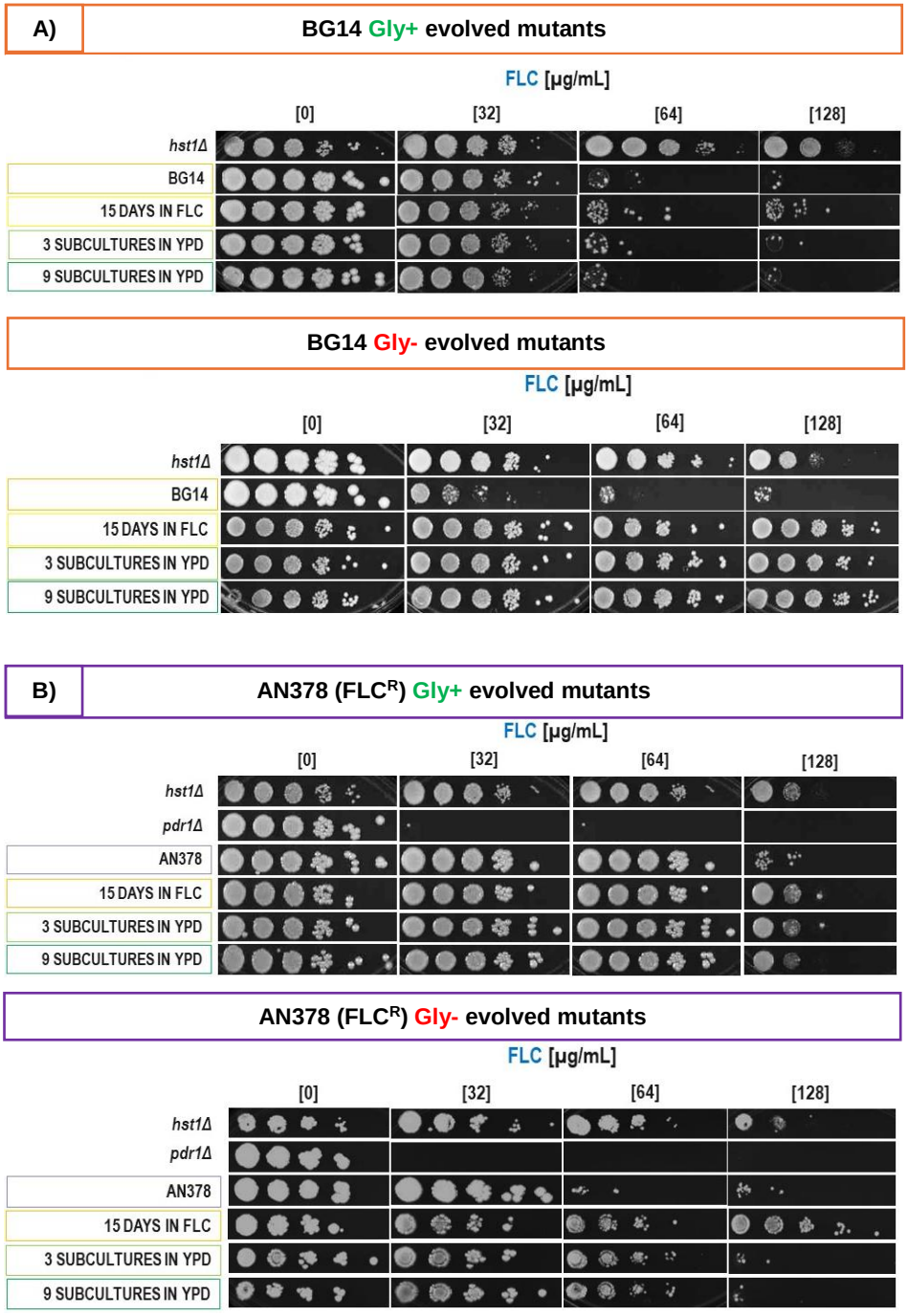
A)
BG14 Gly+ evolved mutants
FLC [µg/mL]
[0]
[32]
[64]
[128]
hst1Δ
BG14
15 DAYS IN FLC
3 SUBCULTURES IN YPD
9 SUBCULTURES IN YPD
BG14 Gly- evolved mutants
FLC [µg/mL]
[0]
[32]
[64]
[128]
hst1Δ
BG14
15 DAYS IN FLC
3 SUBCULTURES IN YPD
9 SUBCULTURES IN YPD
B)
AN378 (FLC^R) Gly+ evolved mutants
FLC [µg/mL]
[0]
[32]
[64]
[128]
hst1Δ
pdr1Δ
AN378
15 DAYS IN FLC
3 SUBCULTURES IN YPD
9 SUBCULTURES IN YPD
AN378 (FLC^R) Gly- evolved mutants
FLC [µg/mL]
[0]
[32]
[64]
[128]
hst1Δ
pdr1Δ
AN378
15 DAYS IN FLC
3 SUBCULTURES IN YPD
9 SUBCULTURES IN YPD

462

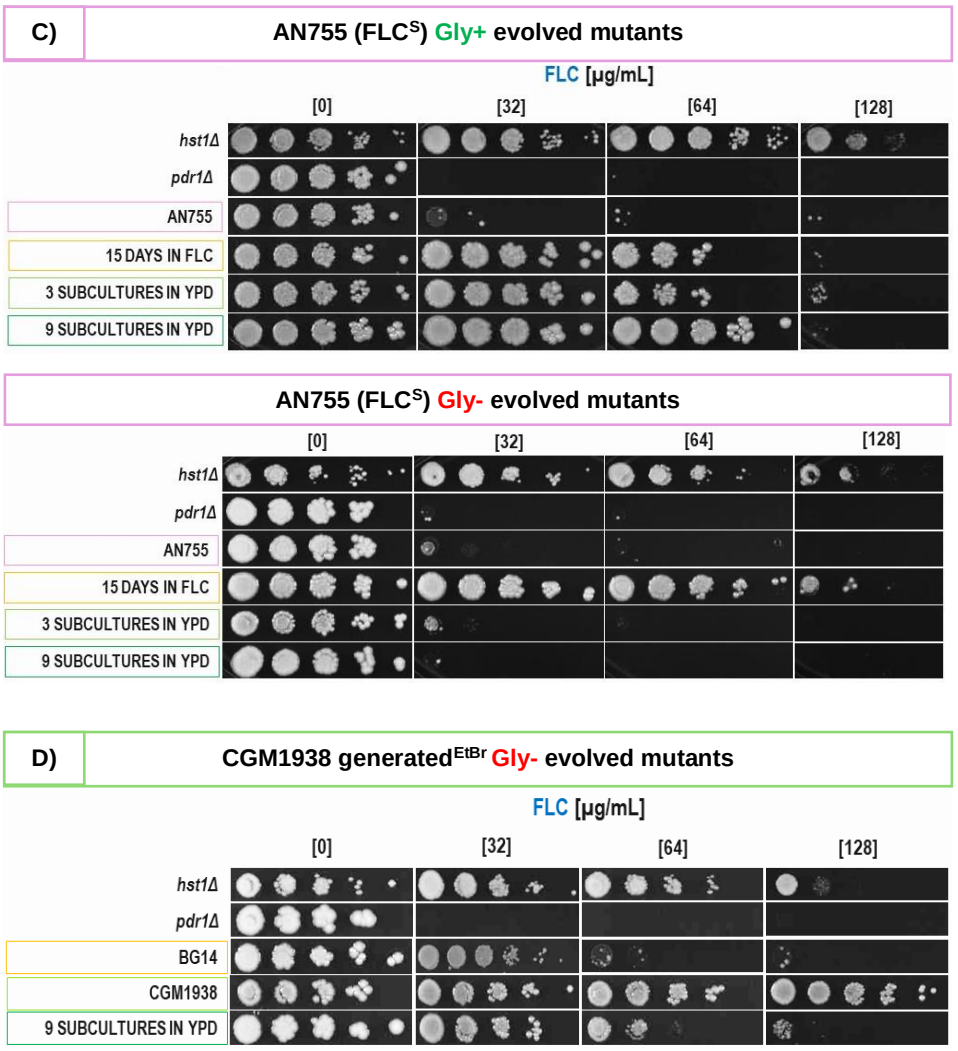

Figure 6. Growth spot assay of evolved mutants at different [FLC] to evaluate the stability of FLC^R phenotype

Spot assay showing the growth of the evolved mutants at several FLC concentrations in **A**, **B**, **C**, and **D**. The evolved mutants were obtained from the BG14, AN378 (FLC^R), AN755 (FLC^S), and CGM1938 (Gly- obtained by exposure to ethidium bromide) genealogies, respectively. In addition, as controls, we included a pdr1Δ strain (FLC^S) and the hst1Δ (FLC^R) strains.

We found that the Gly- phenotype correlates with an unstable acquired FLC^R phenotype in the BG14, CGM1938, AN378 FLC^R, and AN755 FLC^S genealogies. At the same time, Gly+ evolved mutants of these genealogies correlate with a stable acquired resistance phenotype.

Based on the growth spot assay results indicating varying stability of the FLC^R phenotype among Gly- and Gly+ mutants derived from our different genealogies, we decided to elucidate if there are epigenetic regulatory mechanisms that could confer instability of the acquired FLC resistance in these strains.

3.8 Construction of a knockout plasmid (pDC1) targeting the *SET2* gene

A research published by Bhakt et al. (2022) showed that removing the gene encoding a histone methyl transferase, Set2, responsible for mono-, di- and trimethylation of the H3K36 in *C. glabrata* conferred FLC resistance to this mutant at a concentration of 64 µg/mL. Generating the *set2*Δ mutant in our different genetic backgrounds will allow us to study epigenetic mechanisms underlying the reversibility of the acquired FLC resistance in our evolved mutants.

We constructed an integrative knock-out vector pDC1 (see **Table S 2**) derived from pYC44 for the knock-out mutation of the *SET2* gene. This plasmid was engineered to contain the sequences of the 5' and 3' intergenic regions of the *SET2* gene from *C. glabrata*, flanking the nourseothricin resistance (*NAT*^{R}) gene cassette. The *NAT*^{R} cassette contains a 3' UTR sequence of the *CTA1* gene followed by a modified *NAT*^{R} gene driven by the Ashbya gossypii *TEF1* promoter. Flp1 recombinase recognition sites (*FRT*) were incorporated flanking the cassette to enable the excision of the NAT^R and the *CTA1* 3' UTR sequences (Yáñez-Carrillo et al., 2015).

To obtain the fragments 5' and 3' intergenic sequences of the *SET2* gene, we designed a set of primers aligning with the target sequences in *C. glabrata's* genome. These primers were designed to include restriction sites, recognized by *Sac*I-*Bam*HI and *Xho*I-*Kpn*I, respectively, to clone into pYC44 in the corresponding sites and the correct orientation see **Table S 3.** Additionally, a restriction site for *Bsg*I was added to the primers to enable the excision of the 5'*SET2-NAT*-3'*SET2* cassette from pDC1

for recombination by double homologous recombination in the desired strains, see **Figure S 3.**

We generated the *set2Δ* mutants in the background of the BG14, AN378 (FLC^R), and AN755 (FLC^S) strains. These will undergo a microevolution experiment in the presence of FLC and caspofungin, another antifungal class targeting the enzyme 1,3-β-glucan synthase, to study possible epigenetic mechanisms underlying antifungal resistance. We also aim to generate a *set2Δ* mutant in the background of AN376, another clinical isolate that is FLC^S but caspofungin resistant, to include it in the microevolution experiment.

4. Discussion

The results of these studies reveal the complex interplay between mitochondrial function and FLC resistance in *C. glabrata*. The emergence of Gly+ and Gly- mutants upon FLC exposure indicates a multifaceted connection between mitochondrial function and acquired FLC resistance. This suggests that disrupting mitochondrial function may be a resistance strategy employed by *C. glabrata* under FLC pressure. Such adaptability aids the survival and proliferation of *C. glabrata* in various niches (Alves et al., 2020). Further research is needed to understand the specific mechanisms through which these mitochondrial dysfunctions contribute to FLC resistance. It has been proposed that cells with mitochondrial dysfunction signal the nucleus through transcription factor Pdr1, which can be upregulated to increase the expression of ABC efflux pumps, such as Cdr1, thereby expelling FLC from the cells (Gale et al., 2023).

The persistence of the Gly- phenotype in the evolved mutants, as we did not observe any reversibility of the Gly- to Gly+ phenotype for any strain originating from the microevolution experiment, suggests a stable state of mitochondrial dysfunction. This finding aligns with previous studies, including that of Arastehfar et al. (2023), which demonstrated that Gly- strains, subjected to 30 passages in YPD after FLC exposure, remained Gly-, except for one strain. Similarly, Kaur et al. (2004) reported that mutants generated by randomized Tn7 insertions in the *SUV3*, *MRPL4*, and *SHE9* genes exhibited elevated fluconazole resistance due to impaired mitochondrial function. Interestingly, fluconazole-associated petites from the wild-type background showed the capability to revert to respiratory competence, indicating that acquired fluconazole resistance is not always due to the irreversible loss of mitochondrial DNA but rather to a reversible loss of mitochondrial function, suggesting an epigenetic mechanism for switching between respiratory-competent and incompetent states.

Our results suggest that the observed phenotypic stability in evolved mutants may stem from changes in nuclear or mitochondrial DNA induced by selective pressure from FLC exposure, as evidenced by the reduced band intensity of the *COX2* and *COX3* genes. Although azole exposure may not consistently result in total mitochondrial DNA loss, it can damage other mitochondrial components (Siscar-

lewin et al., 2021). Such genomic changes in mitochondrial DNA could be due to gene alterations required for mitochondrial repair or function, leading to errors in mitochondrial DNA replication. This is corroborated by our findings in the staining variations of mitochondrial structure using MitoTracker™ Green FM and the absence of Prx1-GFP fluorescence in Gly- mutants compared to Gly+ mutants.

Furthermore, increased ROS production in Gly- cells may activate stress-response pathways (Briones-Martin-Del-Campo et al., 2014; Garcia-Rubio et al., 2021). Accumulated oxidative stress can impair mitochondrial function by disrupting membrane permeability, the respiratory chain, and mitochondrial DNA integrity, which may limit the cells' ability to revert to a Gly+ phenotype (Peng et al., 2012).

Enhanced ROS production in Gly- cells and the involvement of mitochondrial fission in the release of cytochrome C from mitochondria, which acts as a scavenger of ROS in the cytosol, might explain the differences observed in the staining patterns with MitoTracker™ Red CMXRos (Okamoto et al., 2023). The more localized mitochondrial fluorescence in Gly+ evolved mutants contrasts with the diffuse cytosolic staining in Gly- cells, possibly due to the accumulation of ROS throughout the cell and issues with ROS detoxification. Defects in mitochondrial fission and fusion processes may also hinder mitochondrial DNA inheritance, distribution, and genome integrity, affecting mitochondrial respiratory activity (Osman et al., 2015).

Furthermore, the partial loss of mitochondrial DNA, the observed mitochondrial dysfunction, the diffused mitochondrial staining, and the lack of fluorescence with the tagged Prx1-GFP in Gly- mutants align with findings from a study on the effects of ketoconazole on ergosterol biosynthesis. Cirigliano et al. (2019) reported that *S. cerevisiae* treated with ketoconazole showed reduced ergosterol levels, significant mitochondrial DNA loss, and aberrant mitochondrial morphology. These results indicate that azole exposure in yeasts, such as *S. cerevisiae* and *C. glabrata,* affects mitochondrial membrane composition, leading to structural damage and potentially partial or complete loss of mitochondrial DNA. Altogether, these findings underscore the complexity of mitochondrial dynamics and suggest the need for further investigation into the mitochondrial-to-nuclear DNA ratio and understanding the specific molecular alterations involved.

The spot growth assay revealed variability in the stability of fluconazole resistance across different genetic backgrounds, with Gly- evolved mutants exhibiting unstable resistance in most strain backgrounds (except in the BG14 standard strain). In this genealogy, both selected colonies, Gly+ and Gly-, maintained stable the acquired FLC resistance levels after subcultures without FLC. This might represent a phenotype of the specific selected colony and could not represent a particular phenotype for this population. Specific genetic mutations across different genetic backgrounds may impact the activity of efflux pumps, drug targets, or other resistance-related factors, contributing to the observed variability in resistance stability.

The role of mitochondria extends beyond energy production, as they produce several metabolites related to epigenetic processes, such as NAD+, ATP, alpha-ketoglutarate, and acetyl coenzyme A, which are essential substrates for nuclear transcriptional and epigenetic processes, including chromatin remodeling, histone modification, and nucleosome positioning (Bartelli et al., 2018). Mitochondrial dysfunction could affect epigenetic regulation by limiting S-adenosylmethionine (SAM) availability. SAM, synthesized by methionine adenosyltransferase and dependent on ATP levels, serves as a crucial methyl donor for histone methylation reactions (Mentch et al., 2015). Diminished ATP levels directly impair SAM production, compromising histone methylation processes. This disruption in histone methylation has far-reaching implications, influencing gene expression patterns involved in stress responses and antifungal resistance. Mitochondrial dysfunction could, therefore, have widespread effects on cellular epigenetics, potentially influencing gene expression patterns that confer drug resistance.

Additionally, epigenetic modifications, such as histone modifications, could regulate gene expression associated with drug resistance. Recent research has highlighted the role of histone H3K36-specific methyltransferase Set2 in modulating the expression of the *CgPDR1* gene. In a *Cgset2Δ* mutant, a slight increase in the expression of *PDR1*-network genes has been observed, which may contribute to the decreased fluconazole susceptibility. This underscores the multifaceted regulation of ABC transporter gene expression (Bhakt et al., 2022; Moirangthem et al., 2021; Patra et al., 2022). Set1-dependent azole resistance was linked to azole-induced

transcriptional activation of *ERG* genes, including the azole target-encoding gene *ERG11* (Baker et al., 2021). These variations suggest a complex interaction between mitochondrial function and fluconazole resistance stability, potentially influenced by epigenetic regulatory mechanisms that require additional study.

Overall, the study highlights the intricate genetic, epigenetic, and mitochondrial factors influencing FLC resistance in *C. glabrata* strains exposed chronically to FLC (**Figure 7**). This underscores the importance of adopting a multifaceted approach to investigate and address antifungal resistance. Further research is necessary to elucidate the underlying molecular mechanisms and identify potential therapeutic targets to enhance treatment efficacy.

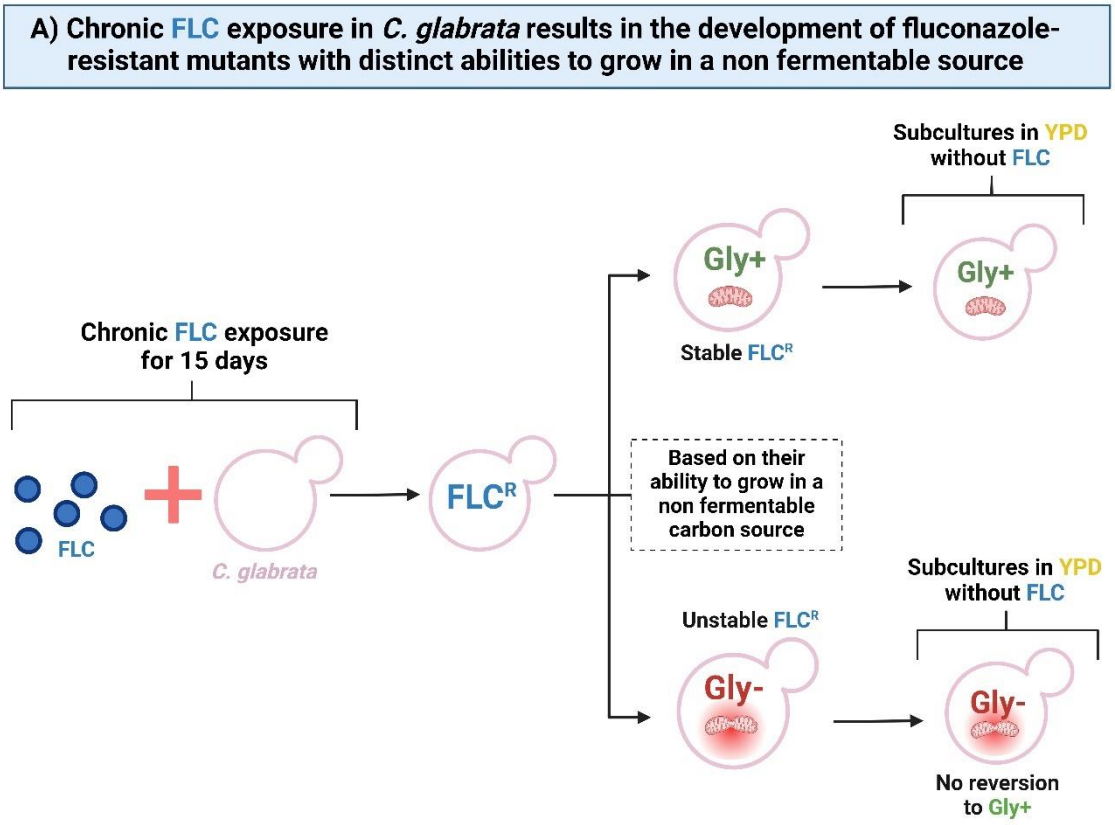
A) Chronic FLC exposure in C. glabrata results in the development of fluconazole-resistant mutants with distinct abilities to grow in a non fermentable source
Subcultures in YPD without FLC
Gly+
Gly+
Stable FLC^R
Chronic FLC exposure for 15 days
FLC
C. glabrata
FLC^R
Based on their ability to grow in a non fermentable carbon source
Subcultures in YPD without FLC
Unstable FLC^R
Gly-
Gly-
No reversion to Gly+

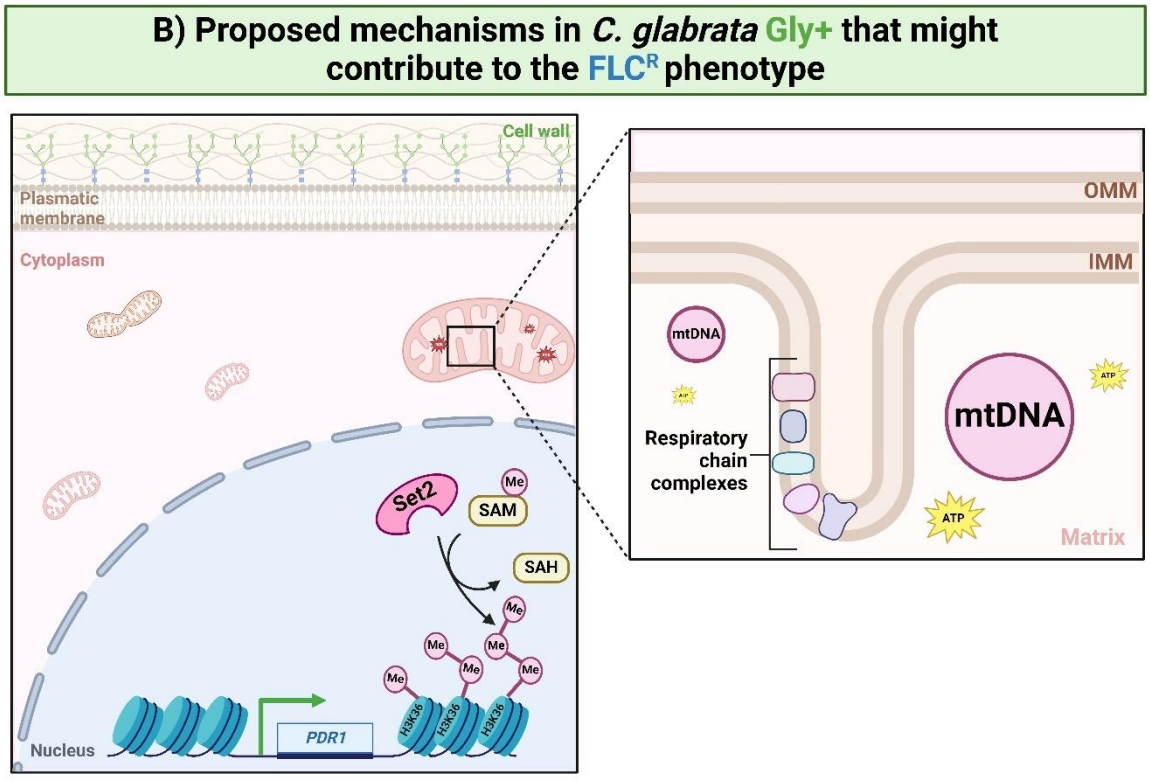
B) Proposed mechanisms in C. glabrata Gly+ that might contribute to the FLC^R phenotype
Cell wall
Plasmatic membrane
Cytoplasm
Set2
Me
SAM
SAH
Me
Me
Me
Me
Me
H3K36
H3K36
H3K36
Nucleus
PDR1
OMM
IMM
mtDNA
ATP
Respiratory chain complexes
mtDNA
ATP
ATP
Matrix

615

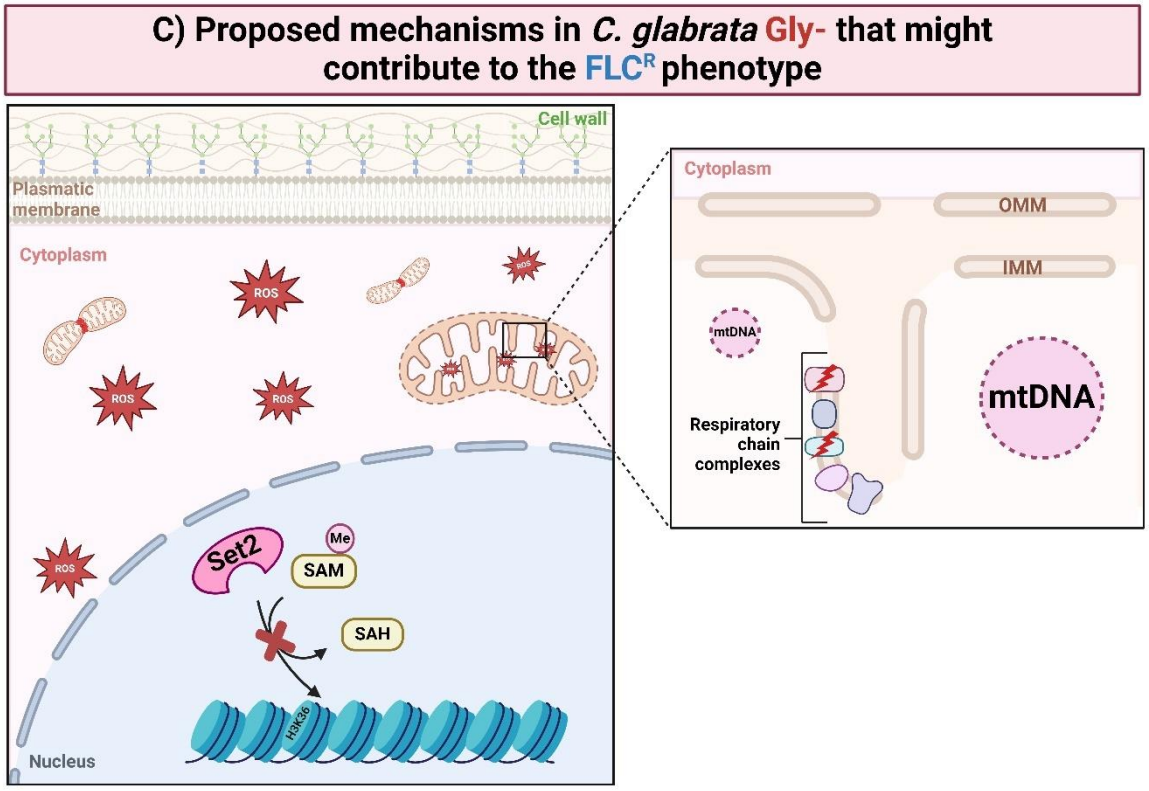

Figure 7. Chronic FLC exposure in C. glabrata and the development of fluconazole-resistant mutants with distinct abilities to grow in non-fermentable carbon sources

A: *C. glabrata* cells were chronically exposed to fluconazole for 15 days. After 15 days of FLC exposure, FLC-resistant (FLC^R) mutants emerge. These mutants are then assessed for their growth ability in non-fermentable carbon sources, classified as Gly+ (capable of utilizing non-fermentable carbon sources) and Gly- (incapable of utilizing non-fermentable carbon sources). Both Gly+ and Gly- mutants are subsequently subcultured in YPD medium without FLC to determine the stability of the FLC^R phenotype and the reversibility of the Gly- phenotype in the absence of FLC. **B: Proposed mechanism in *C. glabrata* Gly+ that might contribute to the FLC^R phenotype.** Functional mitochondria in Gly+ mutants exhibit an intact mitochondrial structure, represented by the undamaged lines of the inner (IMM) and outer (OMM) mitochondrial membranes. This intact structure facilitates ATP production, detoxification of reactive oxygen species (ROS), and maintenance of mitochondrial DNA (mtDNA). ATP production is essential for synthesizing S-adenosylmethionine (SAM), a key methyl donor for the histone methyltransferase Set2. Set2-mediated methylation of histone H3 lysine 36 (H3K36) is crucial for regulating gene expression, including the upregulation of *PDR1*, a gene involved in FLC resistance. Functional respiratory chain complexes and intact mtDNA support the continuous supply of ATP, ensuring effective epigenetic modifications

sustaining the FLC^R phenotype. **C: Impact of mitochondrial dysfunction on histone methylation and gene expression in *C. glabrata.*** This figure illustrates the downstream effects of mitochondrial dysfunction on histone methylation and gene expression. Mitochondrial dysfunction leads to damage in mitochondrial structure, increased ROS production, errors in ROS detoxification, and impaired ATP production, consequently reducing SAM synthesis. Insufficient SAM levels compromise the activity of the histone methyltransferase Set2, resulting in inadequate methylation of H3K36. This can affect chromatin compaction, as Set2-mediated methylation is essential for the transcription of genes, including those involved in antifungal resistance.

5. Conclusions

In this study based on a microevolution experiment, we investigated the stability of the FLC^R phenotype, as well as mitochondrial function and structure in evolved mutants of *C. glabrata*, and found that:

1) Exposing *C. glabrata* strains to chronic FLC resulted in the development of fluconazole-resistant evolved mutants with distinct differences in their ability to grow on glycerol as a carbon source (Gly- / Gly+).
2) Gly- mutants cannot revert to the Gly+ phenotype, indicating a stable mitochondrial dysfunction state.
3) Analysis of mitochondrial DNA indicated potential loss or damage of mitochondrial genes *COX2* and *COX3*, providing insight into the molecular basis of the Gly- persistent phenotype.
4) Using MitoTracker™ Green FM and Mitotracker™ Red CMXRos and fluorescence microscopy, the Gly- mutants exhibit a more diffuse fluorescence signal, suggesting alterations in mitochondrial structure and function compared to the well-defined mitochondria observed in Gly+ strains. Prx1-GFP localization indicated a lack of fluorescence in Gly- evolved mutants, additionally pointing to disruptions in mitochondrial integrity.
5) Our findings on the spot growth assay suggest a correlation between the Gly- phenotype and unstable FLC resistance in the AN378 (FLC^R), AN755 (FLC^S), and CGM1938 genealogies, while Gly+ mutants correlate with stable resistance. The BG14 genealogy presented an exception, where Gly- mutants maintained stable resistance and Gly+ mutants showed instability. These results highlight the complex interplay between genetic background, phenotype, and FLC resistance stability. Furthermore, they suggest that epigenetic regulatory mechanisms could be at play that contribute to the reversibility of acquired FLC resistance.

6. Perspectives

We aim to conduct a microevolution experiment with *set2Δ* mutants across various genetic backgrounds. This will include strains with different innate resistance profiles, such as susceptible-dose dependent resistance, FLC resistance and susceptible, and FLC susceptible but echinocandin resistance.

By exposing these mutants to FLC, a fungistatic agent, we aim to induce a state of growth arrest that may lead to stress-induced genetic instability (Ben-Ami et al., 2016). We will also incorporate caspofungin, a fungicidal agent that targets 1,3-β-glucan synthase and disrupts fungal cell wall synthesis (Spreghini et al., 2012). This approach will allow us to observe gradual adaptations and resistance mechanisms in *C. glabrata* over multiple generations.

We expect to select resistant mutants over time by using sublethal FLC and caspofungin concentrations. This approach will allow the exploration of potential epigenetic changes linked to the evolution of antifungal resistance (Etier et al., 2022). This research may offer valuable insights into the underlying processes contributing to antifungal resistance development.

To further characterize the Gly- phenotype, we intend to construct episomal plasmids expressing proteins localized to specific mitochondrial subcompartments tagged with GFP, RFP, or YFP through translational fusions. We will quantify the mitochondrial-to-nuclear DNA ratio in Gly- compared to Gly+ evolved mutants using qPCR with *COX2* and *COX3* mitochondrial gene primers and the single-copy nuclear gene *CYT1*. In addition, we will employ a series of primers to map segments of the mitochondrial genome, such as *COX1*, *COX2*, *COX3*, and *SSU* genes, to identify potential genetic variations in these sequences in evolved mutants across different points in the microevolution experiment. These target genes were chosen based on recent reports that mutations in their sequences may be implicated in the emergence of the Gly- phenotype (Arastehfar et al., 2023; Helmstetter et al., 2022; Stumpf et al., 2010).

7. References

Alves, R., Kastora, S. L., Gomes-Gonçalves, A., Azevedo, N., Rodrigues, C. F., Silva, S., Demuyser, L., Dijck, P. Van, Casal, M., Brown, A. J. P., Henriques, M., & Paiva, S. (2020). Transcriptional responses of Candida glabrata biofilm cells to fluconazole are modulated by the carbon source. *Biofilms and Microbiomes*, *4*(4), 1–11. https://doi.org/10.1038/s41522-020-0114-5

Arastehfar, A., Daneshnia, F., Hovhannisyan, H., Fuentes, D., Cabrera, N., Quinteros, C., Ilkit, M., Ünal, N., Hilmioğlu-polat, S., Jabeen, K., Zaka, S., Desai, J. V, Lass-flörl, C., & Shor, E. (2023). Overlooked Candida glabrata petites are echinocandin tolerant, induce host inflammatory responses, and display poor in vivo fitness. *American Society for Microbiology*, *14*(5), 1–25.

Baker, K. M., Hoda, S., Saha, D., Georgescu, L., Serratore, N. D., Zhang, Y., Lanman, N. A., & Briggs, S. D. (2021). Set1-mediated histone H3K4 methylation is required for azole induction of the ergosterol biosynthesis genes and antifungal drug resistance in Candida glabrata. *BioRxiv*, *11*, 2021.11.17.469015. https://doi.org/10.1101/2021.11.17.469015

Bartelli, T. F., Bruno, D. C. F., & Briones, M. R. S. (2018). Evidence for mitochondrial genome methylation in the yeast Candida albicans: A potential novel epigenetic mechanism affecting adaptation and pathogenicity? *Frontiers in Genetics*, *9*(MAY), 334277. https://doi.org/10.3389/FGENE.2018.00166/BIBTEX

Bhakt, P., Raney, M., & Kaur, R. (2022). The SET-domain protein CgSet4 negatively regulates antifungal drug resistance via the ergosterol biosynthesis transcriptional regulator CgUpc2a. *Journal of Biological Chemistry*, *298*(10), 102485. https://doi.org/10.1016/j.jbc.2022.102485

Briones-Martin-Del-Campo, M., Orta-Zavalza, E., Juarez-Cepeda, J., Gutierrez-Escobedo, G., Cañas-Villamar, I., Castaño, I., & De Las Peñas, A. (2014). The oxidative stress response of the opportunistic fungal pathogen Candida glabrata. *Revista Iberoamericana de Micología*, *31*(1), 67–71. https://doi.org/10.1016/J.RIAM.2013.09.012

Cirigliano, A., Macone, A., Bianchi, M. M., Oliaro-Bosso, S., Balliano, G., Negri, R., & Rinaldi, T. (2019). Ergosterol reduction impairs mitochondrial DNA

maintenance in S. cerevisiae. *Biochimica et Biophysica Acta - Molecular and Cell Biology of Lipids*, *1864*(3), 290–303. https://doi.org/10.1016/j.bbalip.2018.12.002

Gale, A. N., Pavesic, M. W., Nickels, T. J., Xu, Z., Cormack, B. P., & Cunningham, K. W. (2023). Redefining pleiotropic drug resistance in a pathogenic yeast: Pdr1 functions as a sensor of cellular stresses in Candida glabrata . *MSphere*, *8*(4). https://doi.org/10.1128/MSPHERE.00254-23/SUPPL_FILE/MSPHERE.00254-23-S0004.XLSX

Garcia-Rubio, R., Jimenez-Ortigosa, C., Degregorio, L., Quinteros, C., Shor, E., & Perlin, D. S. (2021). Multifactorial role of mitochondria in echinocandin tolerance revealed by transcriptome analysis of drug-tolerant cells. *MBio*, *12*(4), 1–20. https://doi.org/10.1128/mBio.01959-21

Gomes, F., Palma, F. R., Barros, M. H., Tsuchida, E. T., Turano, H. G., Alegria, T. G. P., Demasi, M., & Netto, L. E. S. (2017). Proteolytic cleavage by the inner membrane peptidase (IMP) complex or Oct1 peptidase controls the localization of the yeast peroxiredoxin Prx1 to distinct mitochondrial compartments. *The Journal of Biological Chemistry*, *292*(41), 17011–17024. https://doi.org/10.1074/JBC.M117.788588

Helmstetter, N., Chybowska, A. D., Delaney, C., Da Silva Dantas, A., Gifford, H., Wacker, T., Munro, C., Warris, A., Jones, B., Cuomo, C. A., Wilson, D., Ramage, G., & Farrer, R. A. (2022). Population genetics and microevolution of clinical Candida glabrata reveals recombinant sequence types and hyper-variation within mitochondrial genomes, virulence genes, and drug targets. *Genetics*, *221*(1). https://doi.org/10.1093/GENETICS/IYAC031

Kaur, R., Castaño, I., & Cormack, B. P. (2004). Functional Genomic Analysis of Fluconazole Susceptibility in the Pathogenic Yeast Candida glabrata: Roles of Calcium Signaling and Mitochondria. *Antimicrobial Agents and Chemotherapy*, *48*(5), 1600. https://doi.org/10.1128/AAC.48.5.1600-1613.2004

Kumar, K., Moirangthem, R., & Kaur, R. (2020). Histone H4 dosage modulates DNA damage response in the pathogenic yeast Candida glabrata via homologous recombination pathway. *PLoS Genetics*, *16*(3). https://doi.org/10.1371/JOURNAL.PGEN.1008620

Mentch, S. J., Mehrmohamadi, M., Huang, L., Thalacker-mercer, A. E., Nichenametla, S. N., Locasale, J. W., Mentch, S. J., Mehrmohamadi, M., Huang, L., Liu, X., Gupta, D., & Mattocks, D. (2015). Histone Methylation Dynamics and Gene Regulation Occur through the Sensing of One-Carbon Article Histone Methylation Dynamics and Gene Regulation Occur through the Sensing of One-Carbon Metabolism. *Cell Metabolism*, *22*, 861–873. https://doi.org/10.1016/j.cmet.2015.08.024

Moirangthem, R., Kumar, K., & Kaur, R. (2021). Two Functionally Redundant FK506-Binding Proteins Regulate Multidrug Resistance Gene Expression and Govern Azole Antifungal Resistance. *Antimicrobial Agents and Chemotherapy*, *65*(6). https://doi.org/10.1128/AAC.02415-20

Okamoto, M., Nakano, K., Takahashi-Nakaguchi, A., Sasamoto, K., Yamaguchi, M., Teixeira, M. C., & Chibana, H. (2023). In Candida glabrata, ERMES Component GEM1 Controls Mitochondrial Morphology, mtROS, and Drug Efflux Pump Expression, Resulting in Azole Susceptibility. *Journal of Fungi*, *9*(2), 240. https://doi.org/10.3390/jof9020240

Osman, C., Noriega, T. R., Okreglak, V., Fung, J. C., & Walter, P. (2015). Integrity of the yeast mitochondrial genome, but not its distribution and inheritance, relies on mitochondrial fission and fusion. *Proceedings of the National Academy of Sciences of the United States of America*, *112*(9), E947–E956. https://doi.org/10.1073/pnas.1501737112

Patra, S., Raney, M., Pareek, A., & Kaur, R. (2022). Epigenetic Regulation of Antifungal Drug Resistance. *Journal of Fungi 2022, Vol. 8, Page 875*, *8*(8), 875. https://doi.org/10.3390/JOF8080875

Peng, Y., Dong, D., Jiang, C., Yu, B., Wang, X., & Ji, Y. (2012). Relationship between respiration deficiency and azole resistance in clinical Candida glabrata. *Federation of European Microbiological Societies*, *12*(6), 719–727. https://doi.org/10.1111/J.1567-1364.2012.00821.X

Scientific, T. (2023). *MitoTracker™ Green FM*. Thermofisher. https://www.thermofisher.com/order/catalog/product/mx/es/M7514

Siscar-lewin, S., Gabaldón, T., Aldejohann, A. M., & Hube, B. (2021). Transient Mitochondria Dysfunction Confers Fungal Cross-Resistance against

Phagocytic Killing and Fluconazole. *MBio*, *12*(3), 1–22.

Spreghini, E., Orlando, F., Sanguinetti, M., Posteraro, B., Giannini, D., Manso, E., & Barchiesia, F. (2012). Comparative effects of micafungin, caspofungin, and anidulafungin against a difficult-to-treat fungal opportunistic pathogen, Candida glabrata. *Antimicrobial Agents and Chemotherapy*, *56*(3), 1215–1222. https://doi.org/10.1128/AAC.05872-11

Stumpf, J. D., Bailey, C. M., Spell, D., Stillwagon, M., Anderson, K. S., & Copeland, W. C. (2010). mip1 containing mutations associated with mitochondrial disease causes mutagenesis and depletion of mt DNA in Saccharomyces cerevisiae. *Human Molecular Genetics*, *19*(11), 2123–2133. https://doi.org/10.1093/hmg/ddq089

Yáñez-Carrillo, P., Orta-Zavalza, E., Gutiérrez-Escobedo, G., Patrón-Soberano, A., De Las Peñas, A., & Castaño, I. (2015). Expression vectors for C-terminal fusions with fluorescent proteins and epitope tags in Candida glabrata. *Fungal Genetics and Biology*, *80*, 43–52. https://doi.org/10.1016/j.fgb.2015.04.020

8. Supplementary figures

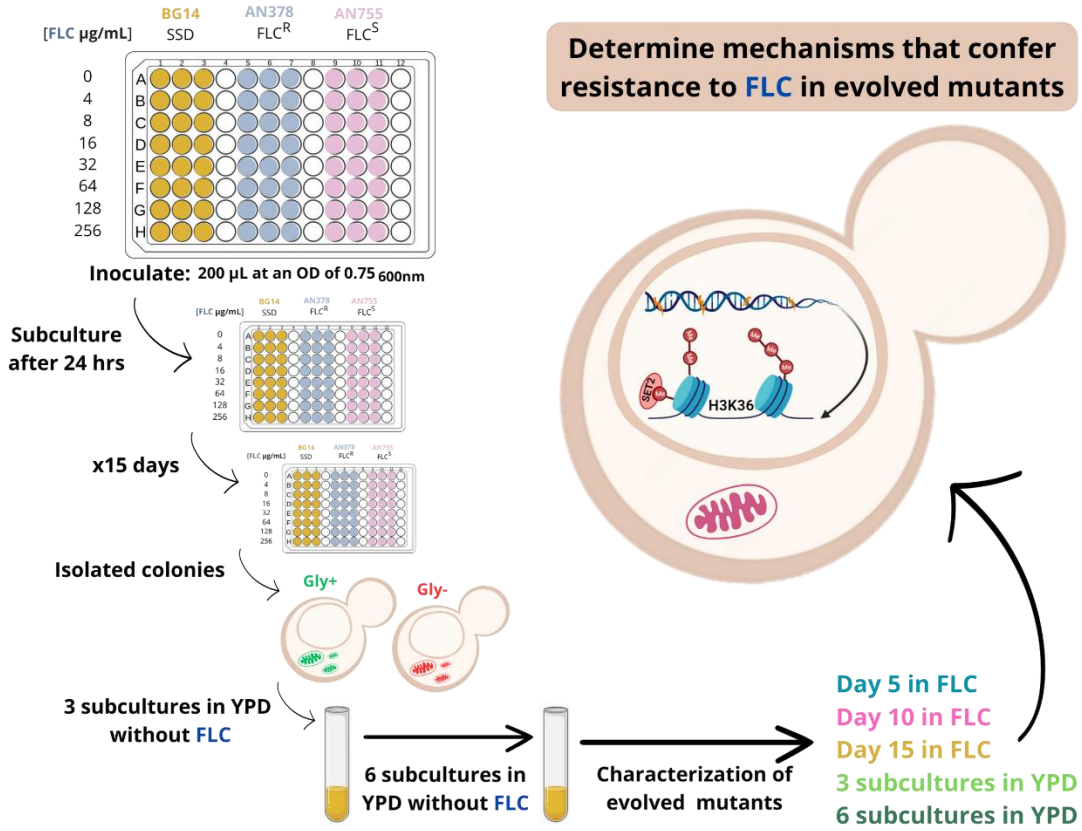

Figure S 1. Microevolution experiment

This figure illustrates the methodology used to investigate the mechanisms of FLC resistance in evolved *C. glabrata* mutants. The experiment involves chronic exposure of C. glabrata cells to varying concentrations of FLC for 15 days. Three strains (BG14, AN378, and AN755) were subjected to incremental FLC treatment, starting with lower concentrations and gradually increasing to 128 µg/mL. After 15 days of FLC exposure, the resultant FLC-resistant mutants were isolated and assessed for their ability to grow in non-fermentable (Gly+) and fermentable (Gly-) carbon sources. Post-FLC exposure, the stability of the FLCR phenotype and the reversibility of the Gly- phenotype were evaluated by subculturing the mutants in a YPD medium without FLC. This subculturing was conducted at two different intervals, three and six times, to assess the durability of the resistance and metabolic phenotypes. The experiment aimed to elucidate the underlying mechanisms conferring FLC resistance in C. glabrata mutants by examining these parameters.

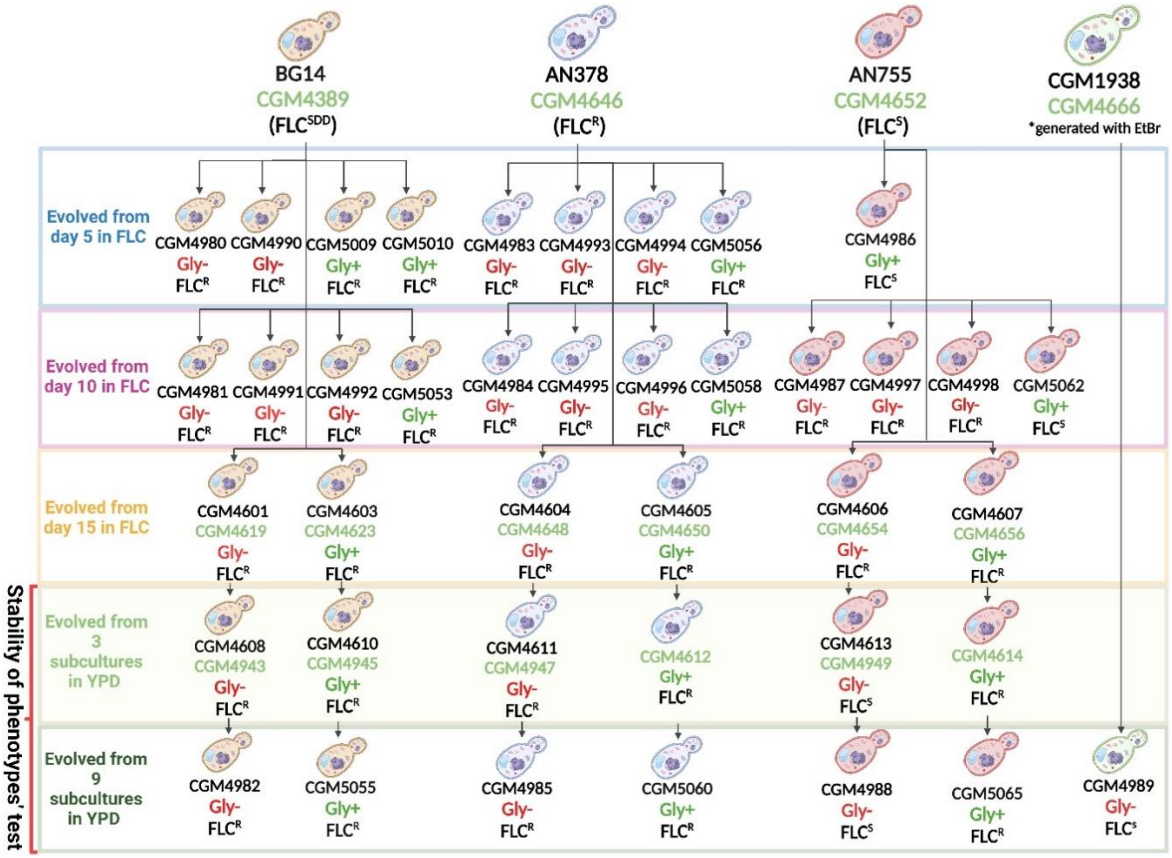

Figure S 2. Genealogy of evolved mutants

Genealogy of *C. glabrata* evolved mutants obtained from the microevolution experiment. Green numbers represent the numbers of the transformed strains with the translational fusion of Prx1-GFP.

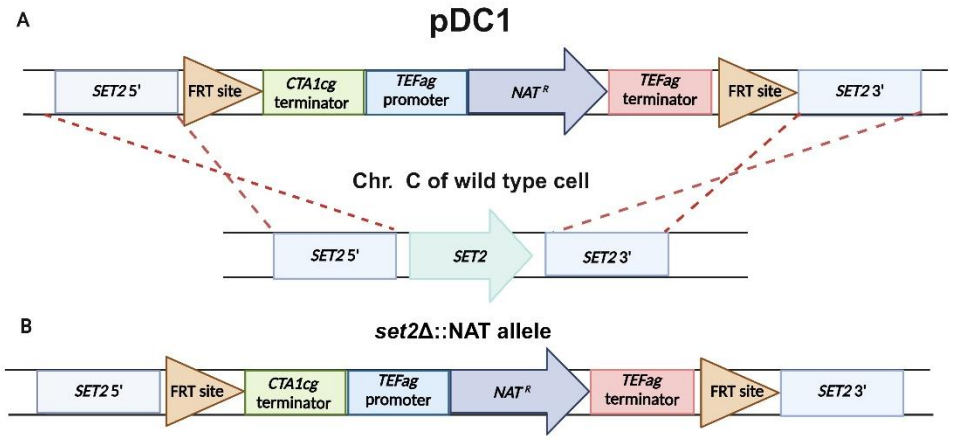

Figure S 3. Schematic representation of double recombination mechanism to generate set2Δ mutants

A: Linearized plasmid with *Bsg*I digestion facilitates homologous recombination of pDC1 cassette. **B**: Allele of *set2Δ* mutant after double homologous recombination.

9. Supplementary Tables

Table S 1. C. glabrata and E. coli strains used in this study

Strain	Parental strain	Plasmid genotype	Phenotype	Reference	Comments
E. coli					
DH10		Genotype: F- *mcrA* Δ*(mrrGhsdRMSG mcrBC) 80dlacZΔM15* Δ*lacX74 deoR recA1 endA1 araD139* Δ*(ara,leu)7697 galU galK U rpsL nupG*		(Calvin & Hanawalt, 1988)	Electrocompetent cells
2944	DH10	Initial Integrative Vector pYC40 (P_{URA3}-URA3-ter_{URA3}, FRT-P_{TEF1}::NAT^R::ter_{TEF1}-FRT)	Amp^R NAT^R $URA3^+$	(Yáñez-Carrillo et al., 2015)	For cloning 3' and 5' end of *SET2*
4768	2944	pAJ77 P_{TEF1}::3UTR_{CTA}::*FRT*	Amp^R NAT^R $URA3^+$	This work	Cloned 3' end of *SET2*
4910	4760	pDC1 P_{TEF1}::3UTR_{CTA}::*FRT*	Amp^R NAT^R $URA3^+$	This work	Cloned 3' and 5' end of *SET2*
4595	4546	P_{PGK1}:: Cg*PRX1-GFP*	Amp^R NAT^R	(Flores-Alvarez, 2023)	Translational fusion of Prx1 with GFP
C. glabrata					
Control strains					
BG14	BG2	*ura3*Δ::Tn903 $G418^R$	URA-	(Cormack et al., 1999)	
pdr1Δ	BG14	*ura3*Δ::Tn903 $G418^R$ *pdr1Δ::hph* – fusion PCR	FLC^S URA-	(Orta-Zavalza et al., 2013)	
hst1Δ	BG14	*ura3Δ*::Tn903 $G418^R$ *hst1Δ*	FLC^R URA-	(Orta-Zavalza et al., 2013)	
Strains isolated from microevolution experiment in the presence of FLC					
BG14 genealogy					
CGM4980	BG14	*ura3*Δ::Tn903 $G418^R$	URA- Gly- FLC^R	This work	Evolved obtained from 5 days in FLC

CGM4990	BG14	*ura3*Δ::Tn903 G418^R	URA- Gly- FLC^R	This work	Evolved obtained from 5 days in FLC
CGM5009	BG14	*ura3*Δ::Tn903 G418^R	URA- Gly+ FLC^R	This work	Evolved obtained from 5 days in FLC
CGM5010	BG14	*ura3*Δ::Tn903 G418^R	URA- Gly+ FLC^R	This work	Evolved obtained from 5 days in FLC
CGM4981	BG14	*ura3*Δ::Tn903 G418^R	URA- Gly- FLC^R	This work	Evolved obtained from 10 days in FLC
CGM4991	BG14	*ura3*Δ::Tn903 G418^R	URA- Gly- FLC^R	This work	Evolved obtained from 10 days in FLC
CGM4992	BG14	*ura3*Δ::Tn903 G418^R	URA- Gly+ FLC^R	This work	Evolved obtained from 10 days in FLC
CGM5053	BG14	*ura3*Δ::Tn903 G418^R	URA- Gly+ FLC^R	This work	Evolved obtained from 10 days in FLC
CGM4601	BG14	*ura3*Δ::Tn903 G418^R pGE316	URA- Gly- FLC^R	(Flores-Alvarez, 2023)	Evolved obtained from 15 days in FLC
CGM4603	BG14	*ura3*Δ::Tn903 G418^R pGE316	URA- Gly+ FLC^R	(Flores-Alvarez, 2023)	Evolved obtained from 15 days in FLC
CGM4608	CGM4601	*ura3*Δ::Tn903 G418^R pGE316	URA- Gly- FLC^R	(Flores-Alvarez, 2023)	Evolved obtained from 3 subcultures in YPD
CGM4610	CGM4603	*ura3*Δ::Tn903 G418^R pGE316	URA- Gly+ FLC^R	(Flores-Alvarez, 2023)	Evolved obtained from 3 subcultures in YPD
CGM4982	CGM4603	*ura3*Δ::Tn903 G418^R	URA- Gly- FLC^R	This work	Evolved obtained from 9 subcultures in YPD
CGM5055	CGM4603	*ura3*Δ::Tn903 G418^R	URA- Gly+ FLC^R	This work	Evolved obtained from 9

					subcultures in YPD
AN378 FLC^R genealogy					
AN378	Blood sample	pFA1	Gly+ FLC^R	Instituto Nacional de Ciencias Médicas y de Nutrición Salvador Zubirán (INCMNSZ)	
CGM4983	AN378		Gly- FLC^R	This work	Evolved obtained from 5 days in FLC
CGM4993	AN378		Gly- FLC^R	This work	Evolved obtained from 5 days in FLC
CGM4994	AN378		Gly+ FLC^R	This work	Evolved obtained from 5 days in FLC
CGM5056	AN378		Gly+ FLC^R	This work	Evolved obtained from 5 days in FLC
CGM4984	AN378		Gly- FLC^R	This work	Evolved obtained from 10 days in FLC
CGM4995	AN378		Gly- FLC^R	This work	Evolved obtained from 10 days in FLC
CGM4996	AN378		Gly+ FLC^R	This work	Evolved obtained from 10 days in FLC
CGM5058	AN378		Gly+ FLC^R	This work	Evolved obtained from 10 days in FLC
CGM4604	AN378	pFA1	Gly- FLC^R	(Flores-Alvarez, 2023)	Evolved obtained from 15 days in FLC
CGM4605	AN378	pFA1	Gly+ FLC^R	(Flores-Alvarez, 2023)	Evolved obtained from 15 days in FLC
CGM4611	CGM4604	pFA1	Gly- FLC^R	(Flores-Alvarez, 2023)	Evolved obtained from 3 subcultures in YPD
CGM4612	CGM4605	pFA1	Gly+ FLC^R	(Flores-Alvarez, 2023)	Evolved obtained from 3

					subcultures in YPD
CGM4985	CGM4611		Gly- FLC^R	This work	Evolved obtained from 9 subcultures in YPD
CGM5060	CGM4612		Gly+ FLC^R	This work	Evolved obtained from 9 subcultures in YPD
AN755 FLC^S genealogy					
AN755	Blood sample	pFA1	Gly+ FLC^S	Instituto Nacional de Ciencias Médicas y de Nutrición Salvador Zubirán (INCMNSZ)	
CGM4986	AN755		Gly+ FLC^R	This work	Evolved obtained from 5 days in FLC
CGM4987	AN755		Gly- FLC^R	This work	Evolved obtained from 10 days in FLC
CGM4997	AN755		Gly- FLC^R	This work	Evolved obtained from 10 days in FLC
CGM4998	AN755		Gly+ FLC^R	This work	Evolved obtained from 10 days in FLC
CGM5062	AN755		Gly+ FLC^R	This work	Evolved obtained from 10 days in FLC
CGM4606	AN755	pFA1	Gly- FLC^R	(Flores-Alvarez, 2023)	Evolved obtained from 15 days in FLC
CGM4607	AN755	pFA1	Gly+ FLC^R	(Flores-Alvarez, 2023)	Evolved obtained from 15 days in FLC
CGM4613	CGM4606	pFA1	Gly- FLC^R	(Flores-Alvarez, 2023)	Evolved obtained from 3 subcultures in YPD
CGM4614	CGM4607	pFA1	Gly+ FLC^R	(Flores-Alvarez, 2023)	Evolved obtained from 3

					subcultures in YPD
CGM4988	CGM4613		Gly- FLC^R	This work	Evolved obtained from 9 subcultures in YPD
CGM5065	CGM4614		Gly+ FLC^R	This work	Evolved obtained from 9 subcultures in YPD
CGM1938 generated with EtBr genealogy					
CGM1938	BG14	*ura3*Δ::Tn903 $G418^R$ pGE316	URA- Gly- FLC^R	Laboratory collection	Obtained with EtBr
CGM4989	CGM4613	*ura3*Δ::Tn903 $G418^R$	URA- Gly- FLC^S	This work	Evolved obtained from 6 subcultures in YPD
***set2Δ C. glabrata* mutants**					
CGM5234	BG14	*set2Δ::*FRT-NAT-FRT	Gly+ NAT^R URA^-	This work	Will undergo microevolution experiment
CGM5235	BG14	*set2Δ::*FRT-NAT-FRT	Gly+ NAT^R URA^-	This work	Will undergo microevolution experiment
CGM5477	CGM1938	*set2Δ::*FRT-NAT-FRT	Gly- NAT^R URA-	This work	Will undergo microevolution experiment
CGM5470	AN378	*set2Δ::*FRT-NAT-FRT	Gly+ NAT^R URA+	This work	Will undergo microevolution experiment
CGM5367	AN755	*set2Δ::*FRT-NAT-FRT	Gly+ NAT^R URA+	This work	Will undergo microevolution experiment
CGM5368	AN755	*set2Δ::*FRT-NAT-FRT	Gly+ NAT^R URA+	This work	Will undergo microevolution experiment

841
842

Table S 2. Plasmids used in this work

Plasmid	Relevant genotype/description	Reference
pGE316	P_{PGK1}*::CgPRX1-GFP.URA3*	Laboratory collection
pFA1	P_{PGK1}*::CgPRX1-GFP.NAT*^{R}	(Flores-Alvarez, 2023)
pYC44	Initial Integrative Vector Amp^R NAT^R $URA3^+$ P_{URA3}-URA3-ter_{URA3}, FRT-P_{TEF1}::NAT^R::ter_{TEF1}-FRT	(Yáñez-Carrillo et al., 2015)
pAJ77	Amp^R NAT^R $URA3^+$ A fragment of 572 bp of 5' IR region of *SET2* gene cloned in X and Y sites in pYC44	This work
pDC1	Initial Integrative Vector pAJ77::$3UTR_{CTA}$::FRT Amp^R NAT^R $URA3^+$ A fragment of 693 bp of 3' IR region of *SET2* gene cloned in X and Y sites in pAJ77. For deletion of *SET2* gene.	This work

846 ***Table S 3. Primers used in this work***

Primer number	Name	Sequence (5´-3´)	Size (bp)
Mitochondrial			
3322	COX2 at 539 Fw	AGGAGCTGATGTTATTCATGATTTT	124
3323	COX2 at 663 Rv	ACATTGTCCATAGAATACTCCTTCT	
3324	COX3 at 606 Fw	TCAGTATTCTATGCTGGTACTGGT	121
3325	COX3 at 727 Rv	AACCTACATGATGAGTAGATGTGAA	
3326	CYT1 at 598 Fw	CAGGCACCAACTACAACCCA	116
3327	CYT1 at 714 Rv	GGCCATTTGAGACGTTGTGG	
Construction of pDC1 integrative plasmid			
3304	SET2 at 612 SacI-BsgI Fw	CAAGGAGCTCTTGTGCAGCTACCAGTGTAGAA GAGAGTGAAT	556
3305	SET2 at 56 BamHI Rv	CTAGGATCCTTTTGGGTGGAACAAATGCTG	
3306	SET2 at +24 XhoI Fw	TCACTCGAGACTTGCTTGATATTCCTGCCA	718
3307	SET2 at +694 KpnI-BsgI Rv	CAAGGGTACCTTGTGCAGATTGACGAGGGATG TTTATTGTTT	
3308	Diag SET2 at -674 Fw	GCACAGAGGGCAATTGATGC	3603
3309	Diag SET2 at +798 Rv	CATGTTGACATGCCAGGACAC	
3310	SET2 at 188 Fw	TAAACCTCGAGGACTGCCTG	598
3311	SET2 at 785 Rv	GCAGCGCCATATCTGTCAAC	
3312	Diag cassette NAT Rv	CTGTCAAGGAGGGTATTCTGGG	1086
3313	Diag cassette NAT Fw	GATGCGAAGTTAAGTGCGCAG	
3336	SET2 at -763 Fw	ACTTGGCTCCAATAGGCCCATGGG	3287
3337	SET2 at +1006 Rv	AGTGTGGGACATTTTGGCAGGAACCG	

847